

STARS


University of Central Florida
STARS

Electronic Theses and Dissertations, 2004-2019

2005

Insulator-insulator Contact Charging As A Function Of Pressure

Michael Hogue
University of Central Florida

 Part of the [Physics Commons](#)

Find similar works at: <https://stars.library.ucf.edu/etd>

University of Central Florida Libraries <http://library.ucf.edu>

This Doctoral Dissertation (Open Access) is brought to you for free and open access by STARS. It has been accepted for inclusion in Electronic Theses and Dissertations, 2004-2019 by an authorized administrator of STARS. For more information, please contact STARS@ucf.edu.

STARS Citation

Hogue, Michael, "Insulator-insulator Contact Charging As A Function Of Pressure" (2005). *Electronic Theses and Dissertations, 2004-2019*. 568.

<https://stars.library.ucf.edu/etd/568>



INSULATOR – INSULATOR CONTACT CHARGING AS A FUNCTION OF PRESSURE

by

MICHAEL DUANE HOGUE
M.S. University of Central Florida, 2000

A dissertation submitted in partial fulfillment of the requirements
for the degree of Doctor of Philosophy
in the Department of Physics
in the College of Arts and Sciences
at the University of Central Florida
Orlando, Florida

Fall Term
2005

Major Professor: Dr. Eduardo Mucciolo

© 2005 Michael Duane Hogue

ABSTRACT

Metal – metal and to an extent metal – insulator contact or triboelectric charging are well known phenomena with good theoretical understanding of the charge exchange mechanism. However, insulator – insulator charging is not as well understood. Theoretical and experimental research has been performed that shows that the surface charge on an insulator after triboelectric charging with another insulator is rapidly dissipated with lowered atmospheric pressure. This pressure discharge is consistent with surface ions being evaporated off the surface once their vapor pressure falls below the saturation vapor pressure. A two-phase equilibrium model based on an ideal gas of singly charged ions in equilibrium with a submonolayer adsorbed film was developed to describe the pressure dependence of the surface charge on an insulator. The resulting charge density equation is an electrostatic version of the Langmuir isotherm for adsorbed surface particles, which describes well the experimental observations.

To my wife Laura and my sons, Alex, Kevin, Ian, and Scott whose encouragement and patience have made this work possible.

ACKNOWLEDGMENTS

I would like to acknowledge NASA, Kennedy Space Center, my co-workers in the Testbeds Branch, my academic advisor, Dr. Eduardo Mucciolo, and my dissertation committee for all their support and advice in this work.

TABLE OF CONTENTS

LIST OF FIGURES	vii
LIST OF TABLES	ix
LIST OF ACRONYMS/ABBREVIATIONS	x
CHAPTER ONE: INTRODUCTION.....	1
CHAPTER TWO: BACKGROUND.....	3
CHAPTER THREE: THEORY	10
CHAPTER FOUR: EXPERIMENT AND DATA	16
CHAPTER FIVE: SUMMARY AND CONCLUSIONS	56
APPENDIX A: DERIVATION OF THE TWO-PHASE EQUILIBRIUM MODEL WITH EFFECTIVE ELECTROSTATIC POTENTIAL.....	62
APPENDIX B: DERIVATION OF THE MODEL EQUATION INCLUDING THE VIBRATIONAL PARTITION FUNCTION.....	70
LIST OF REFERENCES	73

LIST OF FIGURES

Fig. 1: Theoretical Paschen discharge curve for flat aluminum electrodes in air	6
Fig. 2: Schematic diagram of charge relaxation on a polymeric particle.....	7
Fig. 3: Polymers rubbed with PTFE and wool.....	8
Fig. 45: Comparison of the model equation with and without the vibrational partition function.....	13
Fig. 5: Comparison of theoretical values for Paschen's law and the model equation.....	15
Fig. 6: Initial triboelectric experiment apparatus.....	18
Fig. 7: Voltage versus pressure data for PTFE rubbed with a wool wheel.....	19
Fig. 8: Curve fit of HDPE surface charge density versus pressure with the model equation.....	20
Fig. 9: Curve fit of PTFE surface charge density versus pressure with the model equation.....	21
Fig. 10: Redesigned triboelectric apparatus.....	23
Fig. 10A: Triboelectric Series.....	24
Fig. 11: Example of mixed discontinuous and continuous discharge with lowered pressure.....	25
Fig. 12: Example of continuous only discharge with lowered pressure.....	26
Fig. 13: Example of curve fitting for the continuous discharge with pressure.....	27
Fig. 14: Discontinuous discharge for HDPE sample # 6 triboelectrified with PTFE felt.....	30
Fig. 15: Curve fit for polycarbonate data with the model equation PTFE felt experiments.....	31
Fig. 16: Aluminum induction plate with electrical connector.....	32
Fig. 17: Induction charging baseline of HDPE sample # 1 with no lowered pressure.....	33
Fig. 18: Typical discharge for inductively charged polymer sample under lowered pressure.....	34
Fig. 19: HDPE sample # 1 + polarity baseline induction experiment with no pump down.....	36

Fig. 20: HDPE sample # 2 + polarity induction experiment.....	37
Fig. 21: Schematic of the corona charging experiment.....	38
Fig. 22: Corona charge plate.....	39
Fig. 23: HDPE sample # 1 corona charging experiment.....	40
Fig. 24: Corona charging data curve fit for PTFE.....	41
Fig. 25: Nickel sample attached to the rubbing wheel in the triboelectric apparatus.....	43
Fig. 26: PTFE sample # 8 tribocharging with Ni (111) baseline.....	44
Fig. 27: Polycarbonate sample # 8 tribocharging with Cu (111) baseline.....	45
Fig. 28: Example of discontinuous discharge with lowered pressure for HDPE sample # 8 tribocharged with Ni (111).....	46
Fig. 29: Example of continuous discharge with lowered pressure for polycarbonate sample # 9 tribocharged with Cu (111).....	47
Fig. 30: Curve fit results for PTFE samples #'s 8,9, and 10 tribocharged with Ni (111).....	48
Fig. 31: Curve fit results for polycarbonate.....	49
Fig. 32: Stable configuration A for a sodium ion adsorbed on HDPE modeled as C ₅ H ₁₂	52
Fig. 33: Stable configuration B for a sodium ion adsorbed on HDPE modeled as C ₅ H ₁₂	52
Fig. 34: Stable configuration C for a sodium ion adsorbed on HDPE modeled as C ₅ H ₁₂	53
Fig. 35: Stable configuration for a sodium ion adsorbed on PTFE modeled as C ₅ F ₁₂	53
Fig. 36: Stable configuration for a chlorine ion adsorbed on PTFE modeled as C ₅ F ₁₂	54
Fig. 37: Stable configuration for a hydroxide ion adsorbed on HDPE modeled as C ₅ H ₁₂	54
Fig. 38: Stable configuration for a hydroxide ion adsorbed on HDPE modeled as C ₅ H ₁₂	54

LIST OF TABLES

Table 1: Curve fit values of polymer discharge data with the model equation	22
Table 2: Curve fit values of polymer discharge data from the redesigned triboelectric device...	28
Table 3: Curve fit values from polymer discharge data using PTFE as the rubbing wheel.....	31
Table 4: Curve fit values of polymer discharge data for corona charging.....	41
Table 5: Curve fit values of polymer discharge data for metal - insulator tribocharging.....	50
Table 6: Comparison of numerical calculations of ion adsorption energies.....	55
Table 7: Comparison of curve fit values from the triboelectric and corona experiments.....	58

LIST OF ACRONYMS/ABBREVIATIONS

ESPL	Electrostatics and Surface Physics Laboratory
KSC	Kennedy Space Center
PTFE	Polytetrafluoroethylene (aka Teflon [®])
HDPE	High Density Polyethylene
LDPE	Low Density Polyethylene
PVC	Polyvinylchloride
JCI	John Chubb Instrumentation
IPA	Isopropyl Alcohol
NaCl	Sodium Chloride
KCl	Potassium Chloride
ppm	Parts per Million
ESD	Electrostatic Discharge

CHAPTER ONE: INTRODUCTION

The goal of this research is to determine the sources and mechanism of insulator – insulator triboelectric charging, namely whether electrons or ions are involved. This may seem a simple question yet there is much subtle physics and some contention over which charged species is responsible for the charge exchange observed between two insulators. This work will show that the majority of the charge exchange between two insulators is mostly ionic in nature and that the insulator material, morphology, environmental conditions, and history play large roles.

First a summary of previous works on triboelectric charging of insulators with insulators and insulators with metals will be given in Chapter 2. This will detail the works that have been developed to explain insulator triboelectric charging as electron exchange and the problems associated with electron exchange between insulators. Then some experiments will be described that show that the charge density acquired on an insulator is very pressure dependent. This pressure dependency of surface charge will lead to more extensive analysis and experimentation.

To explain the observed pressure dependence of insulator surface charge density, a two – phase equilibrium model will be developed in Chapter 3 by equating the chemical potentials of the adsorbed surface particles and gaseous particles in the atmosphere. The resulting equation will be identified as an electrostatic version of a Langmuir isotherm. Work on including effective electrostatic potentials and the effects of the vibrational partition function will be covered as well. Also, the resulting model equation will be compared to Paschen’s law to show that the discharges with lowered pressure that are observed experimentally are not related to discharges between metal electrodes.

Chapter 4 describes the experimentation performed to provide data for evaluating the validity of the model equation. This chapter is broken into five parts: insulator – insulator triboelectric charging, induction charging, corona charging, metal – insulator triboelectric charging, and a numerical calculation of the adsorption energies of several ions on polymers. The triboelectric experiments using wool and PTFE felt rubbing wheels used eight polymers that span the triboelectric series. The surface charge and pressure data is curve fit to the model equation to determine a value for the adsorption energy of the charged particles.

The induction and corona experiments charge the polymers by known mechanisms (electrons and ions, respectively) using lowered pressure to remove the surface charge density. Comparison of the results of these experiments to the triboelectric experiments will show that ions are mostly responsible for the charge exchange between insulators. The metal – insulator triboelectric experiments charge the polymers by rubbing them with oriented metal samples. This experimentation will show that while electron exchange cannot be ruled out, much of the charge transfer between metals and insulators under ambient conditions is also ionic in nature.

Finally, the theory and experimentation will be discussed and summarized in the concluding Chapter 5. This chapter will describe the results, problems, issues, and potential future work on the triboelectrification of insulators.

Insulator triboelectrification is a major problem on Earth, in space, and on planetary surfaces. Much destruction and loss of life has been caused by the ESD of insulator materials from the explosion of grain silos to the premature detonation of rocket motors. Triboelectric testing of materials is an ongoing program at KSC for all insulator materials used in its facilities, such as plastic sheets, structures, clothing, and flooring, among others.

CHAPTER TWO: BACKGROUND

Charging by metal-to-metal contact is readily understood as an exchange of electrons due to the difference in the metal work functions [1]. Electrons occupying high energy states in a given metal can lower their energy by moving to another metal with unoccupied levels with lower energy. The amount of charge transferred, Q , is given by $Q = VC$, where V is the potential difference and C is the geometry-dependent capacitance of the system. For metal-to-metal contact charging, the above equation can be written as

$$Q = \frac{(\mathbf{f}_A - \mathbf{f}_B)}{q_e} C, \quad (1)$$

where $\mathbf{f}_A - \mathbf{f}_B$ is the difference in the work functions of metals A and B respectively, and q_e is the electron charge (approximately 1.602×10^{-19} Coulombs).

Metal-insulator contact charging was found to be linearly proportional (with some exceptions) to the metal work function when tested with polymers [1,2]. This allowed an effective work function to be assigned to the polymers. Electron transfer is theorized to be between the metal's Fermi level and a localized energy level in the band gap of the insulator [3,1]. These localized energy levels can be formed by impurities, surface states, and defects in the crystal structure. The transferred charge equation would be the same as Eq. (1), except that one of the metal work functions would be replaced by the effective work function of the polymer [4]. Using these insulator work functions, Davies [5] developed a triboelectric series to explain the sign and magnitude of the charge expected between insulator-insulator contacts. Davies provided experimental verification of this and additional data was provided by Stella (unpublished data referenced in [6]) that in general agree with Davies' values.

There are, however, problems with the electron transfer view for metal-insulator charging. Electrons in insulators do not have single energy levels as they do in conductive metals. The energy of an electron in an insulator is a function of its physical position, surface impurities, and the materials' chemical and atomic structure. Thus, the work function for an insulator could only be determined by experiment and might be sample dependent [1]. Other works show that there is not a linear relationship between surface charge and the metal work function unless there are multiple contacts with elastic deformation, resulting in a change in the area of contact [7,8]. However, the common practice is to use the effective work function for insulators to determine the charge exchange after insulator-insulator contact.

A possible mechanism for contact charging between insulators is ion exchange. Surface impurities which can be mostly ionic in nature, will also play a role in the charging of insulators. Ion transfer in metal-insulator charging has been advocated by several researchers [9-11] to account for charge exchange. Ions can exist on the surface of an insulator either in weak bonds due to intermolecular forces while residing in vibrational energy states [2] or as solvated ions in a thin surface water layer [12].

Many materials are hydrophilic and have thin layers of water molecules on their surfaces. The thickness of this water layer varies from several hundred angstroms (\AA) for materials in very humid environments at atmospheric pressure to about 10 \AA for materials in high vacuum chambers [2]. This solid/aqueous interface can be treated as an electrical double layer system with solvated ions in the water that are chemically adsorbed on surfaces. These ions can include Na^+ , Cl^- , OH^- , etc. The net charge on the surface of the solid material would be balanced by an opposite charge of ions in the water layer at the solid/aqueous interface, hence the name electrical double layer [12].

The contact between two surfaces is mostly between the aqueous phase of the surface double layer unless large contact forces are used. If the two electric double layers are at different potentials, then a rearrangement of the distribution of the solvated ions can take place giving each surface a net (and opposite) charge after separation. This electrolytic view of triboelectrification was favored a long time ago by Freundlich [13].

Experiments performed by Matsuyama and Yamamoto [14] measured the charge generated on a metal plate by impact with a polymeric particle. They found that the charge developed on the particle were limited in low pressure by the Paschen limit.

The Paschen discharge limit or Paschen's law was derived to explain the maximum electrical field sustainable in a gas between two metal electrodes [15]. The critical discharge potential is a function of several factors such as the gas species, gas pressure, electrode metal, and electrode separation [16]. A Paschen curve is typically graphed as discharge or sparking potential voltage versus the product of gas pressure and electrode separation. The discharge voltage decreases with pressure to a minimum value because, as pressure decreases, the mean free path between collisions increases, allowing for a greater charged particle kinetic energy to develop. The Paschen curve then increases from the minimum due to a lack of mediating gas atoms to be ionized. An example of a theoretical Paschen curve for flat Aluminum electrodes in air is given in Fig. 1. The Paschen curve represents the maximum strength of an electric field allowed in a gas at the particular set of factors mentioned above. Stronger fields will result in either corona discharge to the air or sparking discharge between the electrodes.

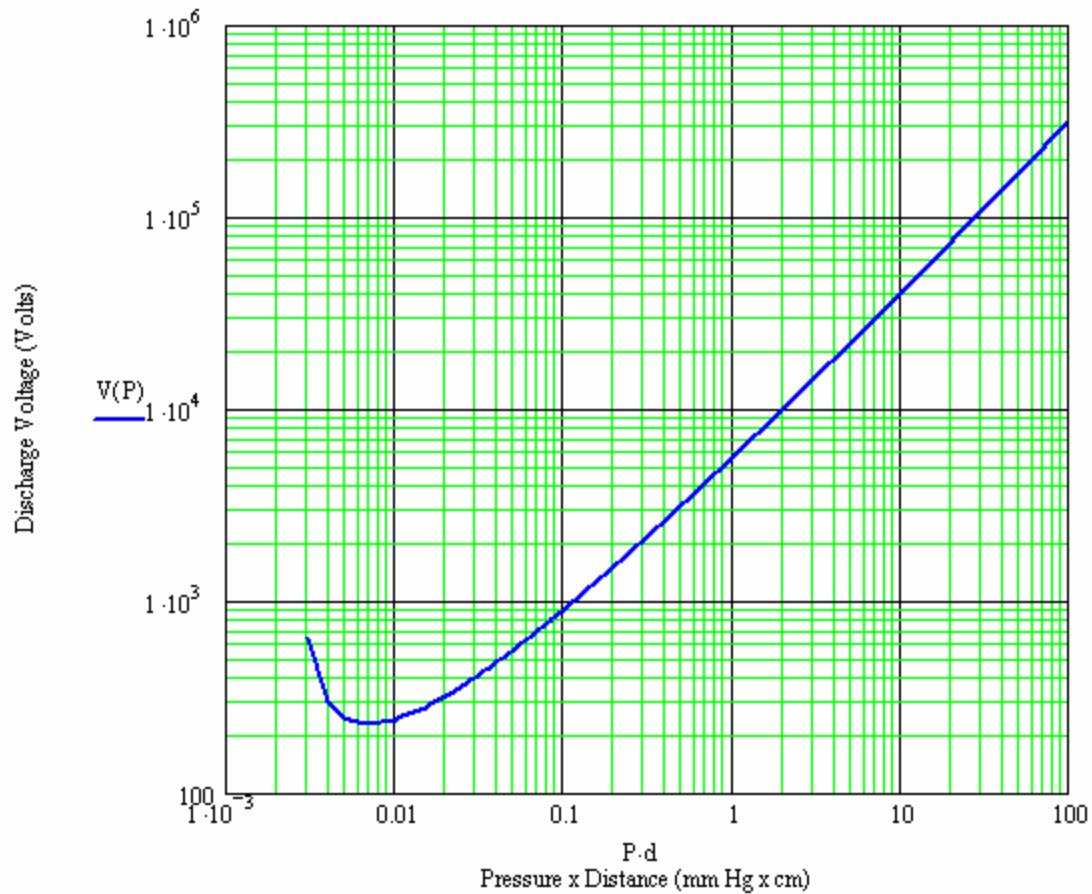


Fig. 1: Theoretical Paschen discharge curve for flat aluminum electrodes in air.

In Matsuyama's experiments [14], charged polymer particles bombard a metal plate and the net charge is measured with a Faraday cup. According to Matsuyama's work, after striking the metal plate, the particle acquires enough charge to exceed Paschen's curve upon separation and thus is forced to lose some charge to gaseous discharge. The remaining charge on the particle is below the Paschen limit but still higher than the initial charge. Figure 2 shows a schematic diagram of this process.

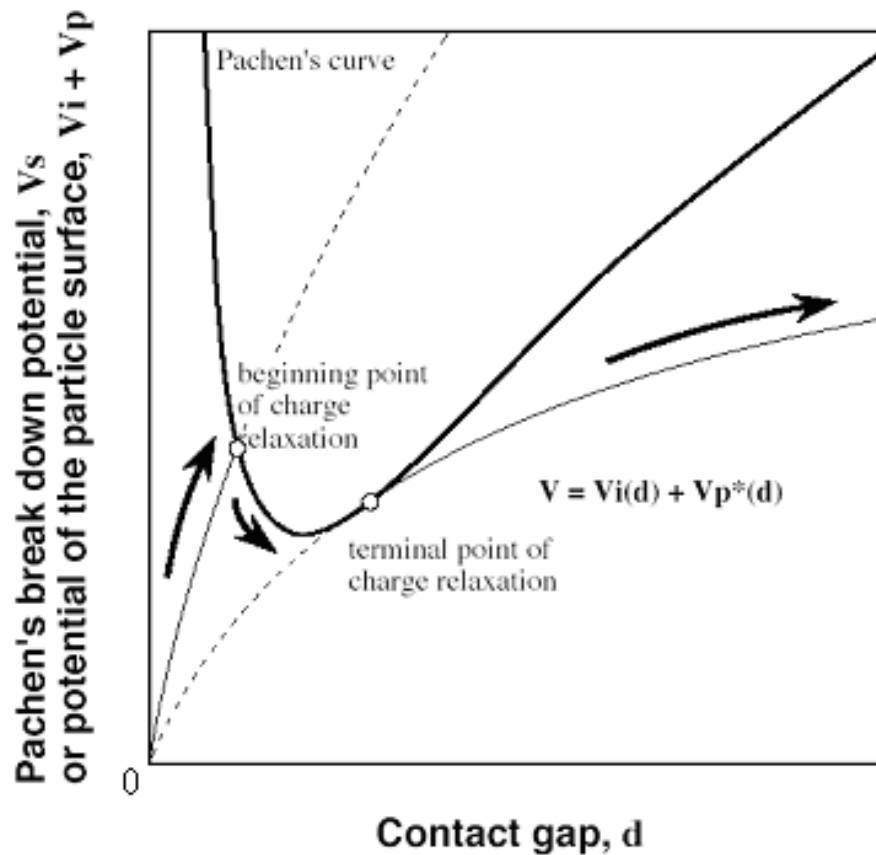


Fig. 2: Schematic diagram of charge relaxation on a polymeric particle after striking a metal plate [14].

This pressure-dependent charging work by Matsuyama guided experiments performed in the ESPL to show the pressure dependence on triboelectric contact charging [17]. Seven polymer insulators that span the triboelectric series were mounted on a wheel inside a bell jar vacuum chamber. These polymers were brought into rubbing contact with wool and PTFE targets, respectively. Electric field data was measured by a John Chubb Instruments JCI 140 CF electrometer at four ambient pressures for each sample material. This data is given in Fig. 3.

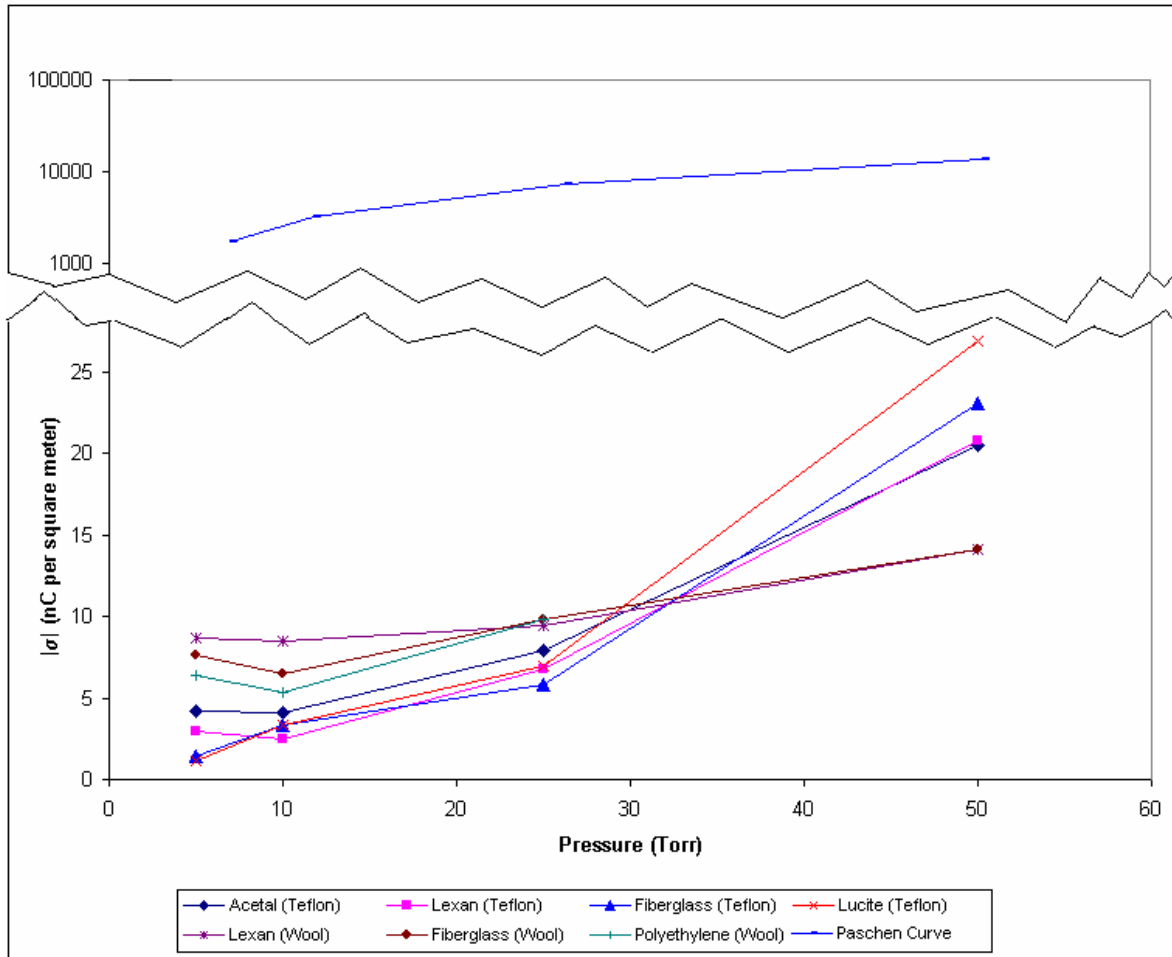


Fig. 3: Polymers rubbed with PTFE and wool showing surface charge dependence on pressure and compared to the Paschen limit for aluminum electrodes in air [17].

As can be seen, the amount of charging decreases with decreasing pressure. Therefore, pressure plays a vital role in determining the residual charge remaining on the surface. For comparison, the Paschen curve for aluminum electrodes in air was plotted in terms of surface charge in Fig. 3 also. This indicates that the low pressure charging effects may be unrelated to Paschen discharge due to the large ($> 100\times$) difference in charging magnitude and difference in

curvature. More on the comparison of Paschen's law to this phenomenon will be discussed in Chapter 3.

The pressure dependence of the surface charge density on an insulator stimulated our work to determine a physical mechanism to explain the phenomenon. Due to the small magnitude of the charging, Paschen discharge or air breakdown did not appear to be viable explanations. A thermodynamic/electrostatic model was developed to explain the surface charge on an insulator as adsorbed surface ions that are removed once the vapor pressure of the ions is reached.

CHAPTER THREE: THEORY

To explain the discontinuous discharge with lowered pressure, a two-phase equilibrium model was developed [18,19,19A,19B]. In this model, the ions responsible for the surface charge density on the insulator surface are an adsorbed submonolayer in equilibrium with a gas of ions in the atmosphere or in a thin surface water layer. The surface is modeled as having localized states with adsorption energy x_0 for the surface ions. The gas phase ions are considered as a vapor of singly ionized particles. Electrostatic potentials in the gas phase are considered in a phenomenological or effective manner by assuming that each particle sees a modified attractive potential towards the surface.

In equilibrium, the chemical potentials of surface and vapor phases are equal [20]. This condition permits the derivation of an equilibrium equation relating the surface charge density, s , with the vapor pressure, P [19]. The resulting equation is

$$s = q_e \frac{N}{A} \frac{1}{\left(\frac{k_B T}{I^3}\right) \frac{e^{-V_0/k_B T}}{P} e^{-x_0/k_B T} + 1}, \quad (2)$$

where q_e is the electron charge, N is the total number of surface adsorption sites, A is the surface area, I is the thermal wavelength (on order of the De Broglie wavelength of a particle of mass m at an energy of $k_B T$), and V_0 is the electrostatic potential energy at the surface. Letting

$s_0 = q_e \frac{N}{A}$ and $P_0 = \left(\frac{k_B T}{I^3}\right) e^{-V_0/k_B T} e^{-x_0/k_B T}$ we can put Eq. (2) into a dimensionless form.

$$\frac{s}{s_0} = \frac{1}{1 + \frac{P_0}{P}}. \quad (3)$$

A few qualitative considerations about Eq. 2 are in order: It represents an electrostatic version of a Langmuir isotherm [21] for ions in equilibrium between an adsorbed surface phase and a gas phase. The Langmuir isotherm describes the dependence of the surface coverage of an adsorbed gas on the pressure of the gas above the surface at a fixed temperature. In this situation the adsorbed particles are taken to be ions. The full derivation of Eq. (2) is given in Appendix A.

It is important to remember that previous work [18] dealt with the derivation of an equation for the surface charge density for an ideal gas of non-interacting particles in equilibrium with an adsorbed monolayer of surface particles. It was found that

$$\mathbf{s} = q_e \frac{N}{A} \frac{1}{\left(\frac{k_B T}{I^3 P}\right)^{-x_0/k_B T} + 1}, \quad (4)$$

which coincides with Eq. (2) except for the $\exp(-V_0/k_B T)$ factor which takes into account the electrostatic screening.

To evaluate V_0 , we need to determine the inverse Debye length, \mathbf{k} , of the system. The Debye or screening length is the characteristic decay length of the surface potential due to the presence of the charge density. This calculation is done in Appendix A. The value of $\exp(-V_0/k_B T)$ obtained from this calculation is approximately 1 making Eq. (2) identical with Eq. (4). This is not an unreasonable result in that the electrostatic forces on an adsorbed and solvated ion in the surface water layer are effectively screened by the presence of the other ions in the water layer and on the surface.

To enhance the fidelity of the model, vibrational energy states of the adsorbed surface ions were also considered. Vibrational modes could be especially important in the case of

hydrophobic materials or low humidity conditions where there is little surface water to solvate the ions.

The adsorbed surface ion is treated as having one degree of vibrational freedom on the surface that can be viewed as a harmonic oscillator with energy

$$E_n = (n + \frac{1}{2})h\nu \quad (5)$$

Where h is Planck's constant, ν is the fundamental frequency of vibration, and n is the integer of the occupied energy state. Including the vibrational partition function in the model equation gives

$$\frac{\mathbf{s}}{\mathbf{s}_0} = \frac{1}{1 + \frac{P_0}{z_{vib}P}} \quad (6)$$

The derivation of Eq. (6) is given in Appendix B. The vibration partition function, z_{vib} , can be determined by performing a numerical calculation of the vibrational frequency of an ion near a surface. Using the code NWChem version 4.6 [22], the vibrational frequency of an adsorbed ion was calculated. For our purposes, we used the case of a singly ionized sodium atom adsorbed on the surface of high density polyethylene (HDPE). The sodium ion is used because it is one of the most common solvated ions. The calculated vibrational frequency in this case is $4.95 \times 10^{12} \text{ s}^{-1}$. At $T = 300\text{K}$, this gives a value for z_{vib} of 1.23. We therefore do not expect vibrational modes to impact the model equation substantially. This can be explained by the fact that at 300 K only the lowest vibrational states are populated with the rest frozen out since $h\nu/k_B \sim 240 \text{ K}$. This was corroborated by performing the curve fit of surface charge density versus pressure as before [18] with Eq. (6), which gives an adsorption energy of $0.36 \pm 0.01 \text{ eV}$ (\pm one standard deviation). For comparison, the value of the curve fit adsorption energy was $0.38 \pm 0.01 \text{ eV}$ based on

experimental data from [19]. These values are within the experimental error of each other. Indeed, upon curve fitting Eq. (6) to the previous experimental data [19], no discernable difference could be noted between this graph and the previous one for HDPE [19]. The theoretical curves are compared in Fig. 4 and show little variation with addition of the vibrational energy partition function.

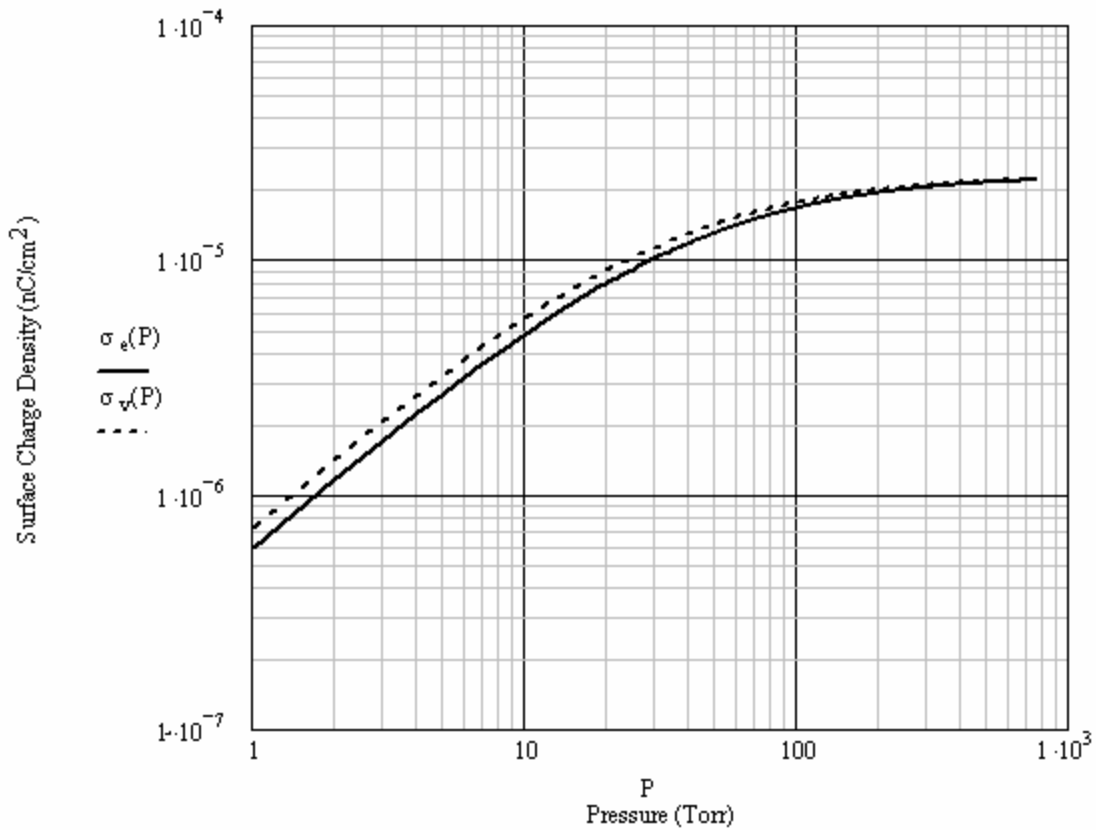


Fig. 4: Comparison of the model equation with (dashed line) and without (solid line) the vibrational partition function.

Let us now discuss possible alternative mechanisms of discharge with lowered pressure. As mentioned in Chapter 2, when electrostatic discharges occur with lowered pressure, the cause is usually attributed to Paschen discharge. Paschen discharge is the spark developed between

two oppositely charged materials when the electrical resistance of the mediating gas between them is overcome by ionization creating a conductive path. This ionization is caused by electrons moving towards the anode and colliding with neutral gas molecules. Paschen's law [16] gives the discharge potential V_s between two metal electrodes as a function of pressure and electrode separation d ,

$$V_s = \frac{V_i P d}{l_{mfp} P_{atm} \left[\ln(Pd) - \ln \left(l_{mfp} P_{atm} \ln \left(1 + \frac{1}{g} \right) \right) \right]}, \quad (7)$$

where V_i is the ionization potential of the ambient gas, l_{mfp} is the mean free path at atmospheric pressure, P is the gas pressure, P_{atm} is atmospheric pressure under standard conditions, and g is the secondary electron emission coefficient of the cathode.

To compare Paschen's law to the model equation, we can rearrange Eq. (7) using Gauss's law to get Paschen's law in terms of surface charge density,

$$\sigma_s = \frac{e_0 V_i P}{l_{mfp} P_{atm} \left[\ln(Pd) - \ln \left(l_{mfp} P_{atm} \ln \left(1 + \frac{1}{g} \right) \right) \right]}, \quad (8)$$

Where σ_s is the surface charge density required on the electrode to cause a discharge. The physical situation used for the comparison is with sodium ions adsorbed with energy 0.4 eV on a surface of area 0.001 m² at a temperature of 300 K. The area is approximately that of the test specimens used in the experimentation and 0.4 eV is in the range of adsorption energies obtained by curve fitting the data to the model equation [19].

For the Paschen's law calculation, aluminum electrodes ($g = 0.35$ [23]) in air ($V_i = 25$ eV) that are 1.0 cm apart are used. At standard atmospheric conditions, $l_{mfp} = 10^8$ m and $P_{atm} =$

101,300 Pa.. Fig. 5 is a graph of the surface charge density versus pressure comparing Paschen's law and the model equation.

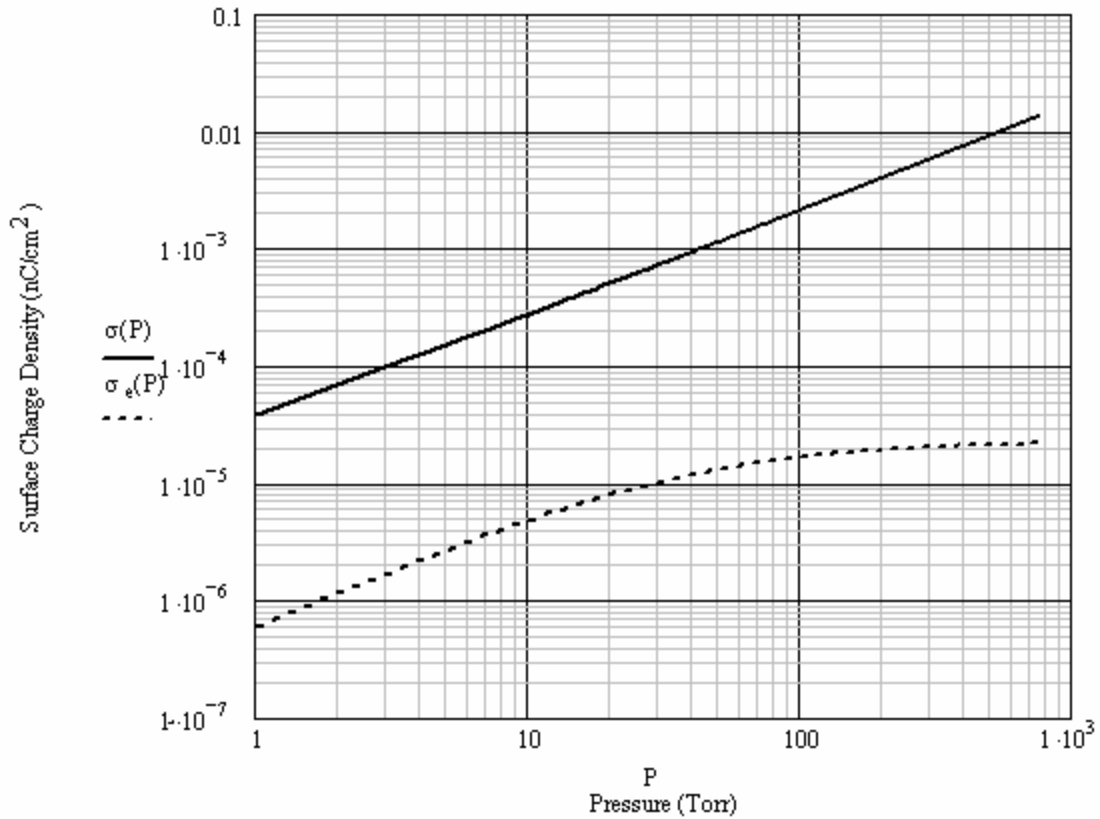


Fig. 5: Comparison of theoretical values for Paschen's law and the model equation

As can be observed from Fig. 5, Paschen discharge is about two orders of magnitude above the theoretical curve for the model equation. Experimental data fits well to the model equation [19] but not to Paschen's law. Therefore the discontinuous discharge with pressure noted in References [18] and [19] cannot be Paschen discharge.

CHAPTER FOUR: EXPERIMENT AND DATA

Part 1: Insulator – Insulator Triboelectric Experiments

To study insulator-insulator contact charging, an experimental triboelectric rubbing apparatus was devised. The experimental apparatus was placed in a bell jar vacuum chamber so that pressure could be lowered after charging. Triboelectric charging of the specimens was achieved using a wool rubbing wheel powered by a small DC electric motor. A John Chubb Instrumentation electrometer, model JCI 140, was used to measure the electric field generated by rubbing the polymers. The JCI 140 is a field mill type electrometer that uses a grounded, rotating plate (chopper) that alternately shields and exposes a sense plate. As the Sense Plate is exposed to the Field, the field induces ground currents as it attracts or repels charge from the Sense Plate. As the sense plate is shielded from the field, the induced charge drains away. So the chopper plate induces an AC ground current which is proportional to electric field strength. A Faraday cup was used to measure the charge on the wool wheel immediately after rubbing. A Faraday cup is a grounded metal container usually open on one end. The metal walls intercept the field lines of charged objects placed into the cup. The resulting current is then read by the instrument and converted to charge. The charge on the wool wheel should be approximately equal and opposite in sign from the charge measured on the polymer sample. This was done to check the accuracy of the JCI 140. The first series of experiments were performed using a manual push rod to place the spinning wool wheel against the specimen. The wool wheel was then deposited by the push rod into the Faraday cup. This test set up is shown in Fig. 6.

Commercially available polymer sheets were used as a source for test specimens. These polymers include high density polyethylene (HDPE), low density polyethylene (LDPE), polycarbonate, polyvinylchloride (PVC), and PTFE (Teflon[®]). Each polymer sheet (0.16 cm thick) was cut into five rectangular 3.8 cm × 7.6 cm specimens. The specimens were cleaned with soap and water, rinsed with deionized water, and then rinsed again with isopropyl alcohol (IPA). The specimens were then allowed to air dry before being sealed in plastic bags.

A polymer specimen was placed in the test apparatus and rubbed with the wool wheel for approximately 7 seconds[†]. The wool was then withdrawn and placed in the Faraday cup. The chamber vacuum pump was started immediately after the rubbing wheel was withdrawn to lower the pressure. Voltage versus pressure measurements were recorded using a Labview[™] data acquisition program loaded on a laptop PC. The chamber took approximately five minutes to fully pump down. Typical final pressures obtained were about 1- 2 Torr using a roughing vacuum pump.

[†] This time seemed to be a good compromise between acquiring sufficient charge on the sample without damaging the surface.

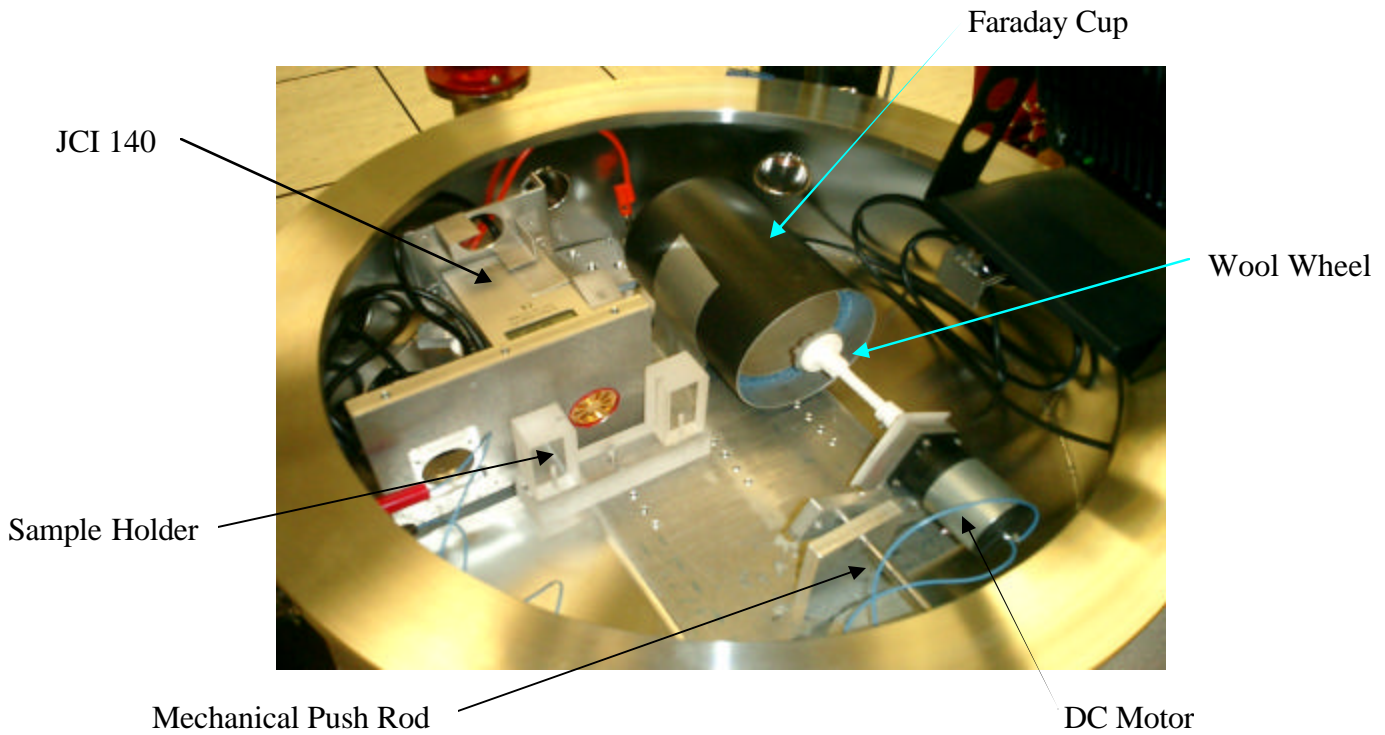


Fig. 6: Initial triboelectric experiment apparatus.

The measured voltage from the surface decreased in a discontinuous, stair-step fashion. The corner points of the discharge data can be approximated as equilibrium points prior to surface discharge. As we will argue later in Chapter 5, this is not exactly accurate. The corner points after the discharge better reflect equilibrium conditions. Nevertheless, the prior data points provide approximately the same fitting parameters. Figure 7 gives an example of the discontinuous discharge for PTFE. Surface charge density was determined by using the surface area of the sample that is effectively measured by the JCI 140 and the distance of the JCI140 from the sample. The resulting experimental data (equilibrium corner points) was curve fit to the model equation (Eq. 3) using a data analysis software called Igor Pro v. 4.01 by Wavemetrics, Inc. Two parameters, the total number of surface adsorption sites, N , and the adsorption energy, χ_0 , were allowed to float or vary in the curve fitting. Examples of the curve fits are given in

Figs. 8 and 9. Table 1 gives the curve fit values of N and x_0 obtained for the polymer samples. In this table, N is total number of occupiable surface sites on an area of 7 cm^2 (approximate area of rubbing on the sample) and is dimensionless.

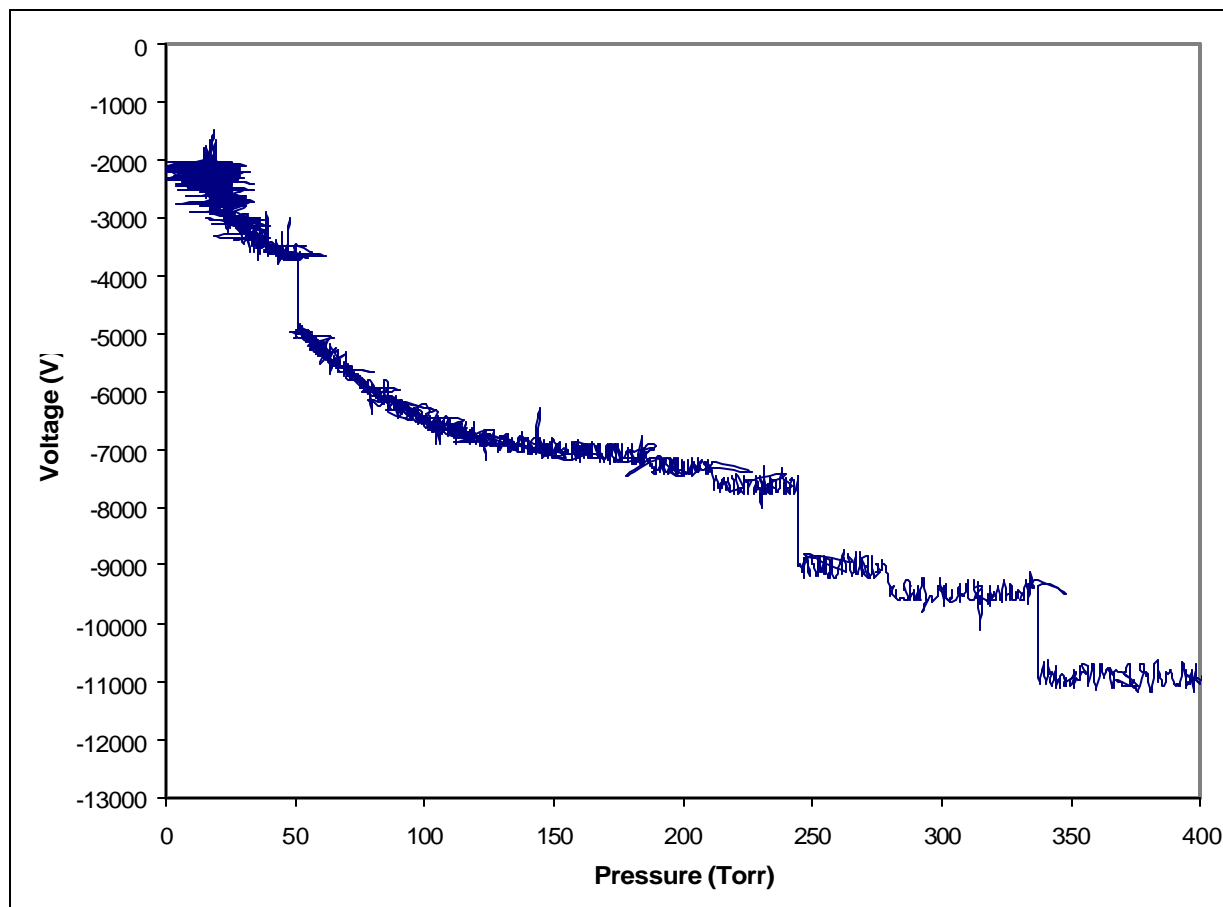


Fig. 7: Voltage versus pressure data for PTFE rubbed with a wool wheel. Time increases as pressure decreases.

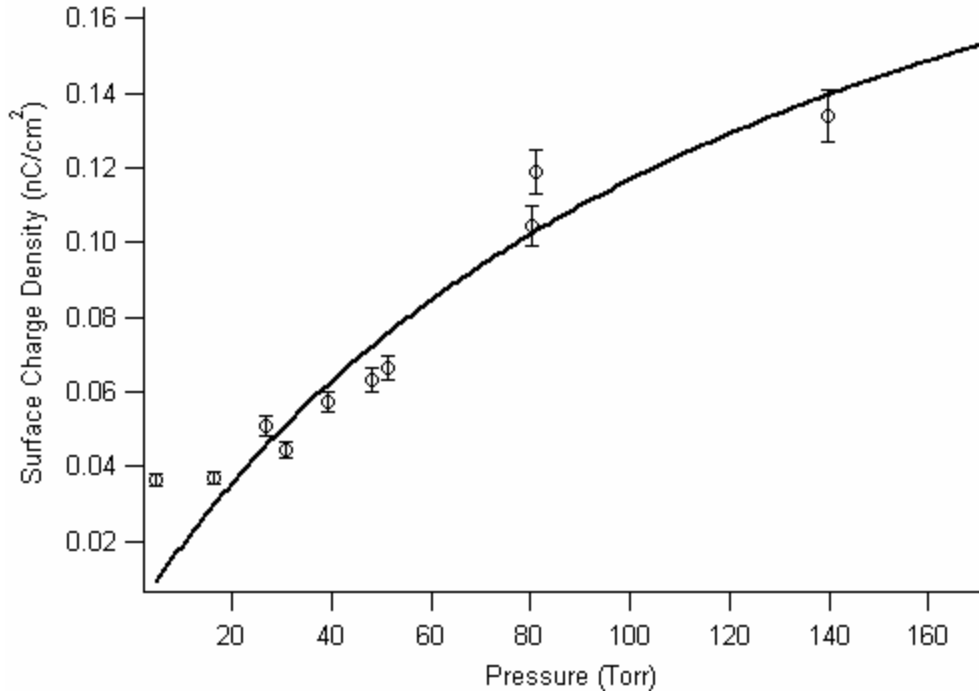


Fig. 8: Curve fit of HDPE surface charge density (wool tribocharging) versus pressure with the electrostatic Langmuir isotherm model equation.

To improve the fidelity of the triboelectric experiments, the triboelectric test apparatus shown in Fig. 6 was redesigned to include two x-y linear motor stages to position the dc rubbing motor/rubbing wheel assembly. This new experimental set-up allowed more precise rubbing time, rpm control, and contact force to be applied to the polymer samples. A new LabviewTM data acquisition program was written for control of these parameters. This new experimental set-up is shown in Fig. 10. Ten new test samples each were fabricated from HDPE, LDPE, PTFE, PVC, Styrene, Polycarbonate, Nylon 66, and Nylon MD. The new polymer samples were cleaned as before prior to the start of experimentation.

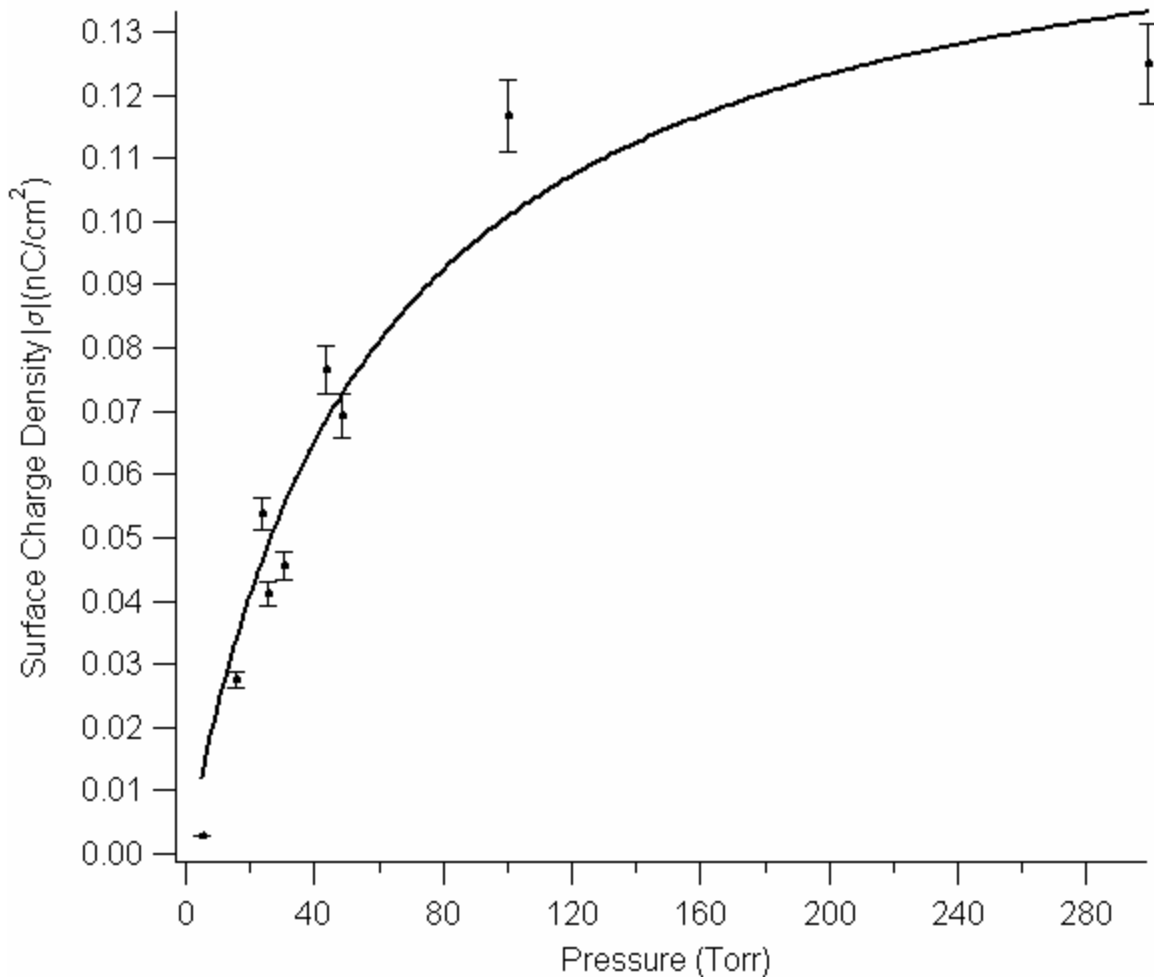


Fig. 9: Curve fit of PTFE surface charge density (wool tribocharging) versus pressure with the electrostatic Langmuir isotherm model.

Table 1
 Curve Fit Values of Polymer Discharge Data with the Model Equation. Range values given are plus and minus one standard deviation.

Polymer	$N (\times 10^{10})$	x_0 (eV)
Polycarbonate	8.88 ± 0.43	-0.40 ± 0.01
HDPE	1.202 ± 0.226	-0.37 ± 0.01
LDPE	0.7 ± 0.07	-0.39 ± 0.01
PTFE	1.783 ± 0.288	-0.35 ± 0.01
PVC	23.36 ± 1.29	-0.35 ± 0.01

Triboelectric experiments were performed on the samples with wool rubbing wheels that were changed out between materials. Data was converted from a .txt file to EXCEL for initial analysis and graphing. Results of these new triboelectric experiments showed that not only did the polymers discharge discontinuously and both discontinuously with continuous parts as before (see Fig. 7) but there were also instances of continuous only discharge with pressure. Examples of these types of discharge are shown in Figs. 11 and 12. In continuous discharge curves, data points were taken along the curve and curve fitted together with data from the corner points.

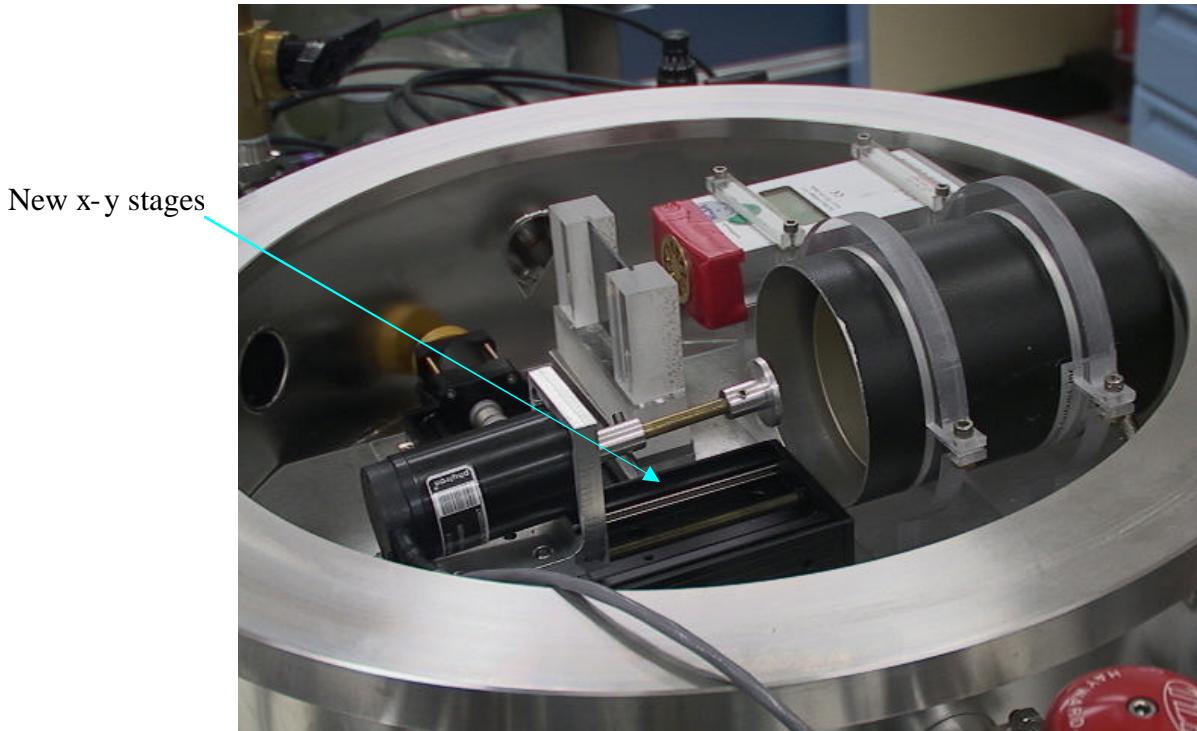


Fig. 10: Redesigned triboelectric apparatus showing new x-y motion stages.

The continuous discharge that occurred in several experiments appears to follow an electrostatic Langmuir isotherm which curve fits well to the model equation. An example of the curve fitting for continuous discharge is shown in Fig. 13. Curve fit results for N and x_0 for these triboelectric experiments are summarized in Table 2. In Chapter 5 we will provide a possible explanation of this behavior.

Also noted in these experiments is that the Nylon and Nylon MD samples did not appreciably charge against wool. This is likely due to Nylon's place in the triboelectric series relative to wool. The triboelectric series is a list of materials based on the sign of the charge due to triboelectrification between any two materials, going from positive at the top of the list to negative at the bottom. In other words, if material A is above material B in the list then upon

rubbing them together A would charge positive and B negative. A triboelectric series is shown in Fig. 10A [24].

+ POSITIVE END OF SERIES

- asbestos
- glass
- nylon
- wool
- lead
- silk
- aluminum
- paper
- cotton
- steel
- hard rubber
- nickel & copper
- brass & silver
- synthetic rubber
- orlon
- saran
- polyethylene
- Teflon (PTFE)
- silicone rubber

- NEGATIVE END OF SERIES

Fig. 10A: Triboelectric series from Ref. [24].

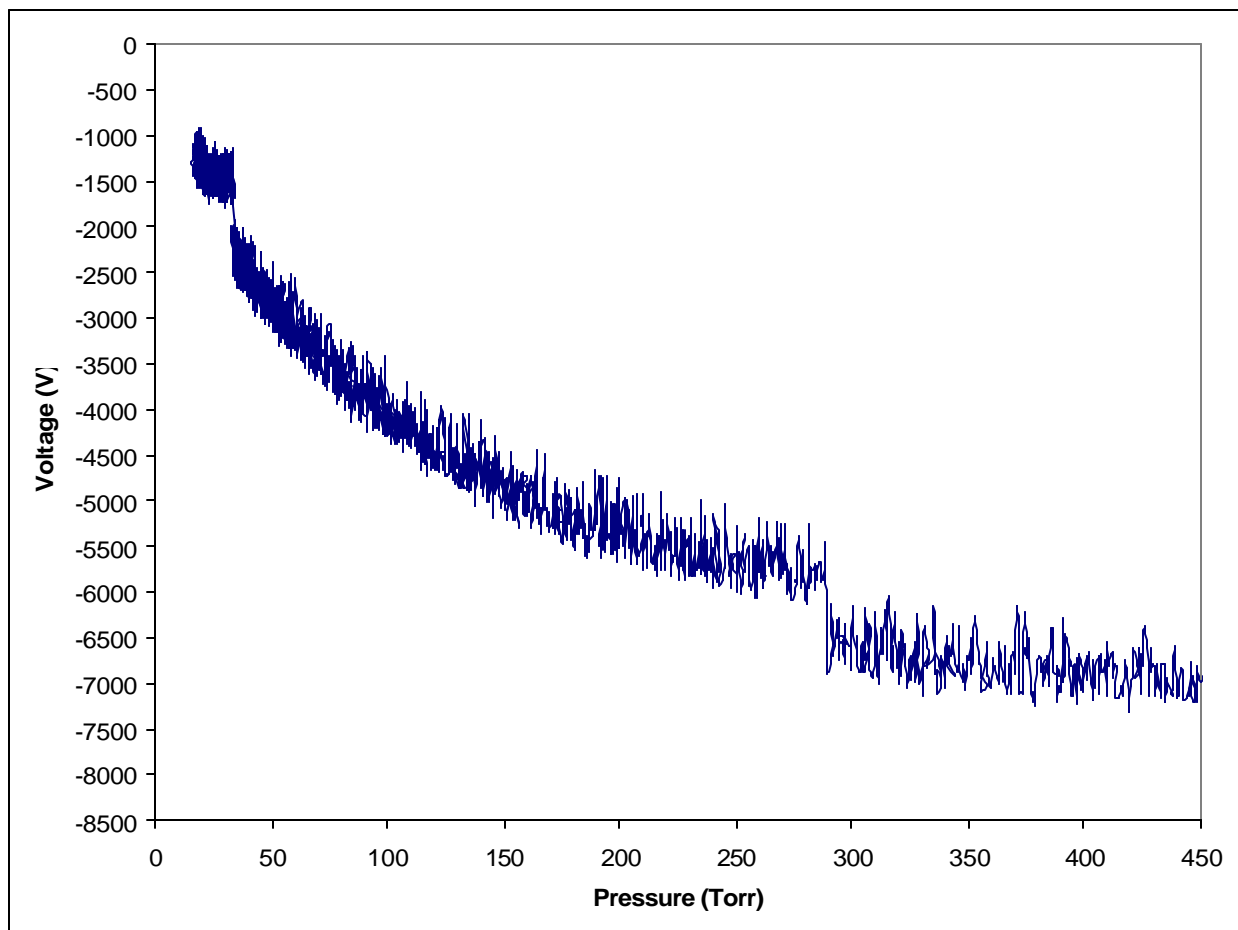


Fig. 11: Example of mixed discontinuous and continuous discharge with lowered pressure. PVC Sample #3

Wool is near the top of the triboelectric series so it will charge most materials negative after triboelectric contact with them. This is the case for all the test polymers except for Nylon.

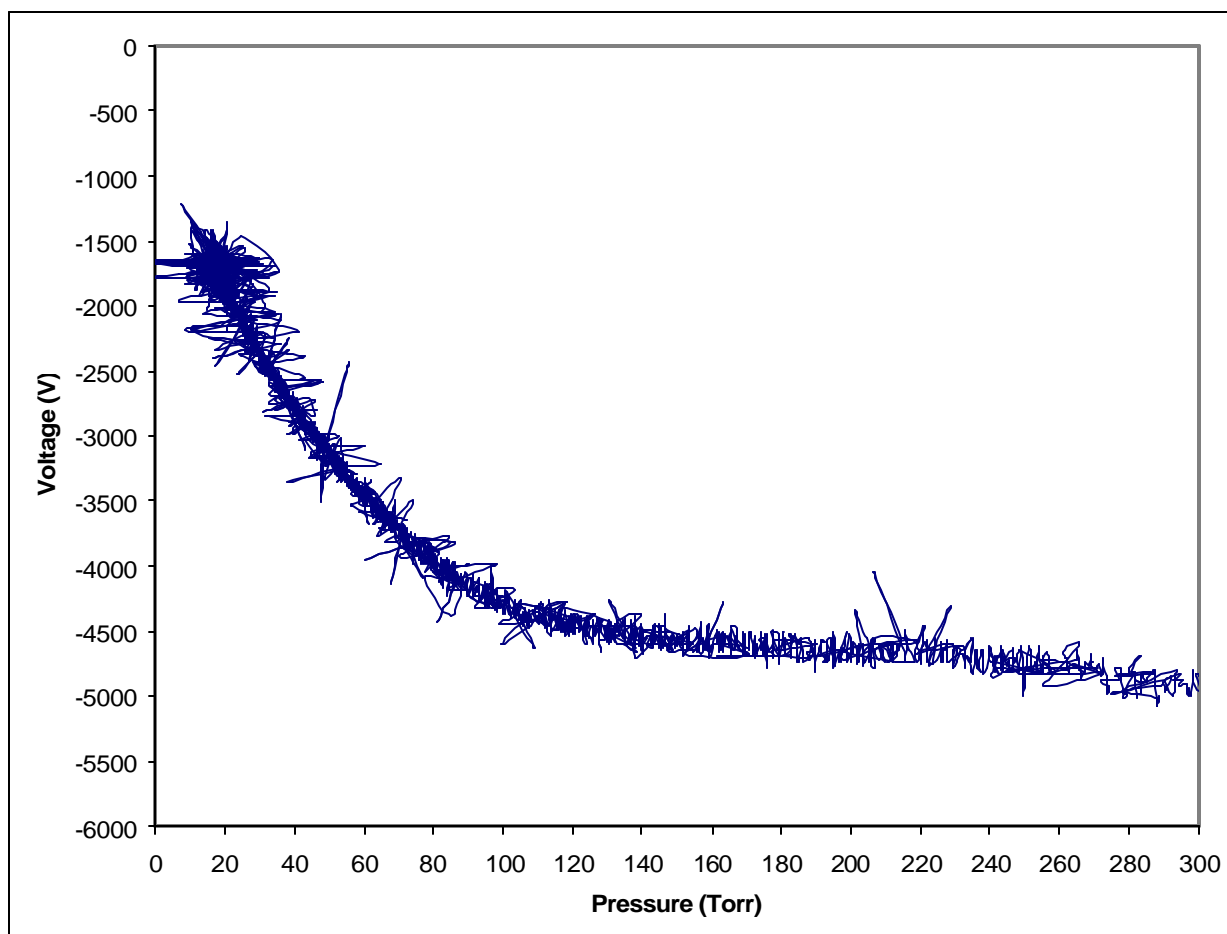


Fig. 12: Example of continuous only discharge with lowered pressure. Polycarbonate Sample 2.

On most triboelectric series, Nylon is positioned just above wool [24]. This should give Nylon a positive charge upon rubbing wool. The data obtained by rubbing wool against Nylon in the experimental apparatus was so small that it was lost in the noise background and the sign of any surface charge could not be determined. The relative position of one material to another on the triboelectric series is not known to imply any magnitude differences in the amount of tribocharging. This lack of significant charge transfer for the wool/Nylon triboelectric experiments remains unexplained physically. One hypothesis to explain the wool/Nylon charging observed is that the low charging was caused by the hydrophilic nature of both wool

and Nylon. Materials on the positive end of the triboelectric series are more hydrophilic than those on the negative end like Teflon, which is strongly hydrophobic. Large surface water layers adsorbed on both wool and Nylon could have mitigated the charge exchange between the two materials. However, other explanations such as conductive additives in the commercially obtained Nylon could not be ruled out.

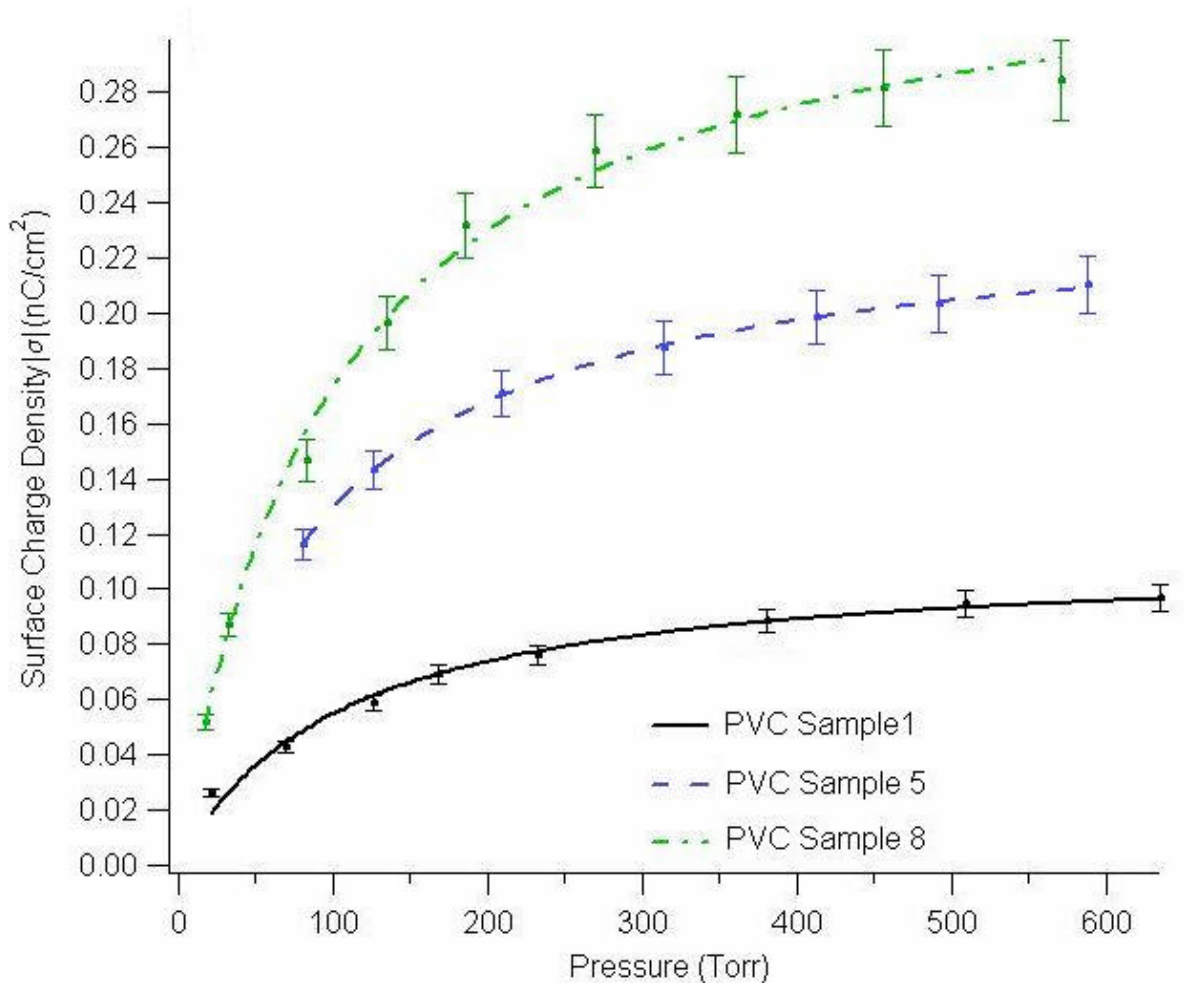


Fig. 13: Example of curve fitting for the continuous discharge with pressure. This is also an example of how different samples of the same material can vary triboelectrically.

Table 2

Curve fit values of polymer discharge data from the redesigned triboelectric apparatus with the model equation. Range values given are plus and minus one standard deviation.

Polymer	$N (\times 10^9)$	x_0 (eV)
HDPE	5.96 ± 0.53	-0.47 ± 0.01
LDPE	6.09 ± 0.77	-0.48 ± 0.01
PTFE (samples #1 & 2)	4.79 ± 0.44	-0.42 ± 0.01
PTFE (samples #3-10)	27.9 ± 3.6	-0.40 ± 0.01
Polycarbonate (corner points)	1.21 ± 0.16	$-0.46 \pm \begin{smallmatrix} 0.01 \\ 0.02 \end{smallmatrix}$
Polycarbonate (sample #1)	2.18 ± 0.06	-0.490 ± 0.003
Polycarbonate (sample #2)	0.85 ± 0.02	$-0.470 \pm \begin{smallmatrix} 0.002 \\ 0.003 \end{smallmatrix}$
Polycarbonate (sample #3)	0.313 ± 0.004	$-0.490 \pm \begin{smallmatrix} 0.002 \\ 0.001 \end{smallmatrix}$
Polycarbonate (sample #9)	0.675 ± 0.006	-0.480 ± 0.001
Styrene	14.2 ± 0.7	-0.46 ± 0.01
PVC (Corner Points)	14.2 ± 1.5	-0.44 ± 0.01
PVC (sample #1)	4.96 ± 0.18	-0.450 ± 0.003
PVC (sample #5)	10.5 ± 0.1	-0.450 ± 0.001
PVC (sample #8)	15.1 ± 3.5	-0.450 ± 0.002

The adsorption energies between some samples of the same material, like PTFE in table 2, varied by about twice the amount (~ 0.02 eV) of the standard deviation (0.01 eV) returned from the curve fit calculation. This shows the effect of slightly different amounts of ions and

contaminants on individual samples. It is also a good indication of the lower bound of the experimental accuracy.

It should be noted that physically the adsorption or desorption of surface particles is not a reversible process. Charge cannot be placed back on the surface by repressurizing the system although mathematically it is allowable. This effect has been verified by continuing to measure the surface charge of test samples after the test chamber has been allowed to come back up to atmospheric pressure and no restoration of surface charge was noted. In the case of the discontinuous discharges, apparently a critical state of charge density and pressure is reached preceding an avalanche of charged particles leaving the surface. This almost instantaneous relaxation of surface charge to the environment is a result of a combination of many factors such as pressure, charged particle species, temperature, properties of the surface material, and surface morphology. A more thorough discussion is postponed to Chapter 5.

To determine if the rubbing material used to tribocharge the polymer samples had any effect on the experimental results, a sample of PTFE felt was also utilized. PTFE is near the bottom of the triboelectric series and should charge the polymers positive and this was indeed observed in the experiments. The PTFE felt was tested against samples of HDPE, LDPE, PTFE, and polycarbonate. As with the wool tribocharging experiments, discharge with lowered pressure was characterized by discontinuous stair-step discharges, continuous discharges, or some combination of both. An example of the discontinuous discharge with pressure using PTFE felt is shown in Fig. 14. Corner and curve points were curve fitted against the model equation as before in the wool – polymer triboelectric experiments. An example of this curve fitting is shown in Fig. 15. Values of the adsorption energy, χ_0 , are around -0.45 eV, which

agree well with the adsorption energy values obtained using wool. The results for N and χ_0 using the PTFE felt as the rubbing wheel material are given in Table 3.

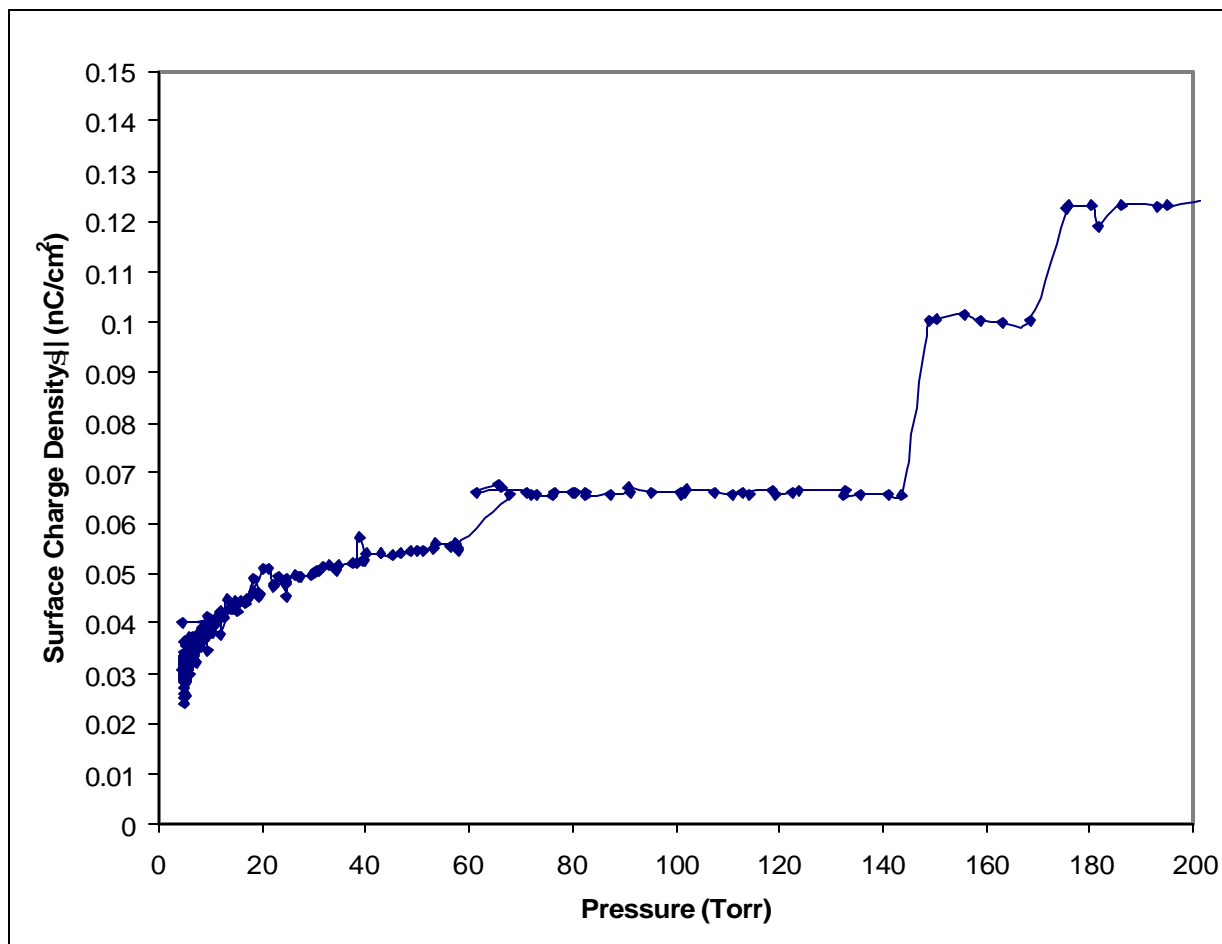


Fig. 14: Example of discontinuous discharge with pressure for HDPE sample # 6 triboelectrified with PTFE felt.

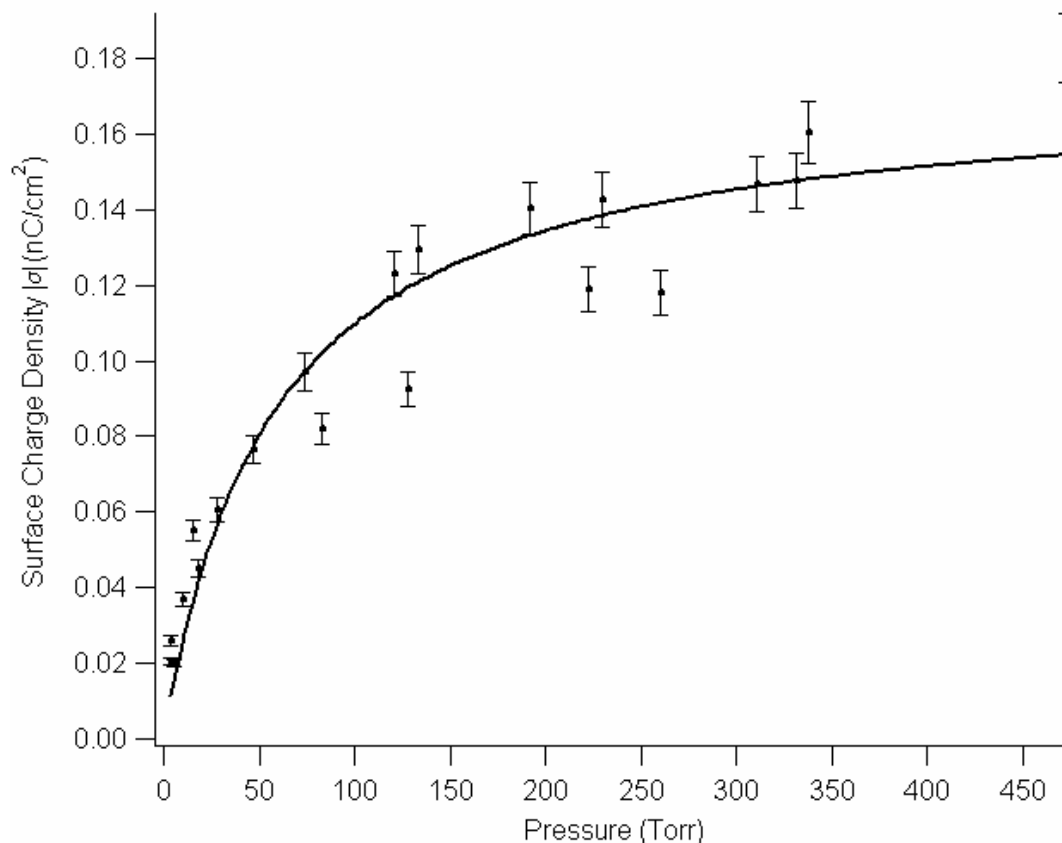


Fig. 15: Curve fit for polycarbonate data with the model equation from the PTFE felt triboelectric experiments.

Table 3

Curve Fit Values from polymer discharge data with the model equation using PTFE felt as the rubbing wheel material. Range values given are plus and minus one standard deviation.

Polymer	$N (\times 10^9)$	x_0 (eV)
HDPE (samples #5 – 7)	6.46 ± 0.94	-0.46 ± 0.01
LDPE (samples #5 – 7)	3.45 ± 0.25	-0.49 ± 0.01
PTFE (sample #5)	5.42 ± 0.14	-0.450 ± 0.002
PTFE (samples #6 & 7)	3.16 ± 0.24	-0.45 ± 0.01
Polycarbonate (samples #5 – 7)	7.65 ± 0.46	-0.46 ± 0.01

Part 2: Induction Experiments

Induction charging occurs when the surface of a material comes in contact with a charged metal plate and electrons are added or removed from the surface depending on the polarity of the charged plate. We have performed such an experiment to help elucidate the nature of the charge carrier involved in the triboelectric polymer charging. Samples # 1 – 4 of HDPE, LDPE, PTFE, and polycarbonate test specimens were used in these experiments. Sample # 1 of each polymer was inductively charged but not exposed to lowered pressure for a baseline to compare to the other three polymers that were inductively charged and exposed to lowered pressure. A 1/16" thick Aluminum plate was cut approximately to polymer sample size and polished. This plate is shown in Fig. 16.

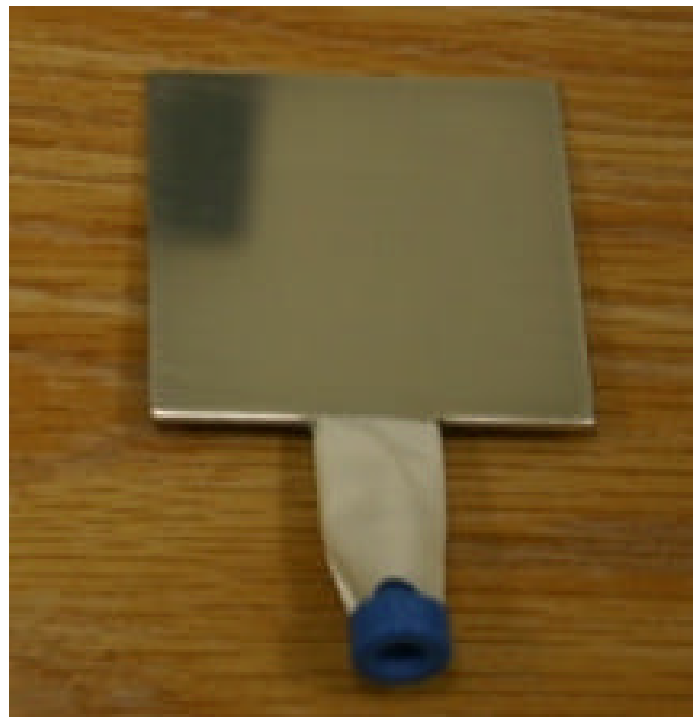


Fig. 16: Aluminum induction plate with electrical connector.

A Keithley model 247 power supply (0 – 3000 V dc) with adjustable polarity was used to supply the voltage to the induction plate. The induction plate was placed in a light, non-rubbing contact with the polymer sample and a voltage of approximately - 2000 V was applied for approximately 15 – 20 seconds. An example of a baseline, no pump down experiment is shown in Fig. 17. In this figure, the voltage increase caused by the charge on the induction plate is shown by the steep peak. The removal of the induction plate causes the voltage to drop rapidly to a low point and then recover somewhat. The slight recovery in voltage is attributed to the response time of the JCI140F catching up with the rapid removal of the induction plate.

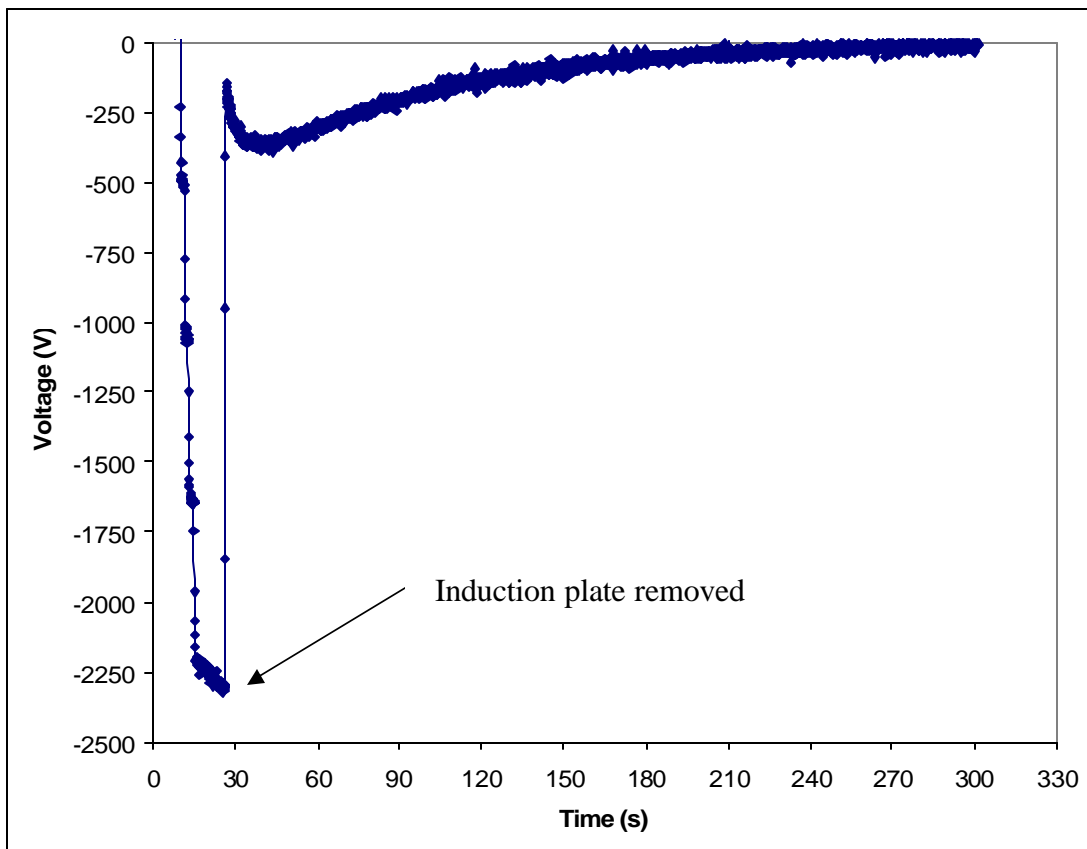


Fig. 17: Induction charging baseline of HDPE sample # 1 with no lowered pressure. Negative polarity was used.

In this experiment, negative polarity was used from the power supply. Subsequent experiments with lowered pressure, after the removal of the induction plate, show that the slow air diffusive charge decay noted in Fig. 17 comes to a halt. This loss of charge decay is explained as the removal of air ions that would normally neutralize the surface electrons or holes. An example of this data along with pressure data is shown in Fig. 18.

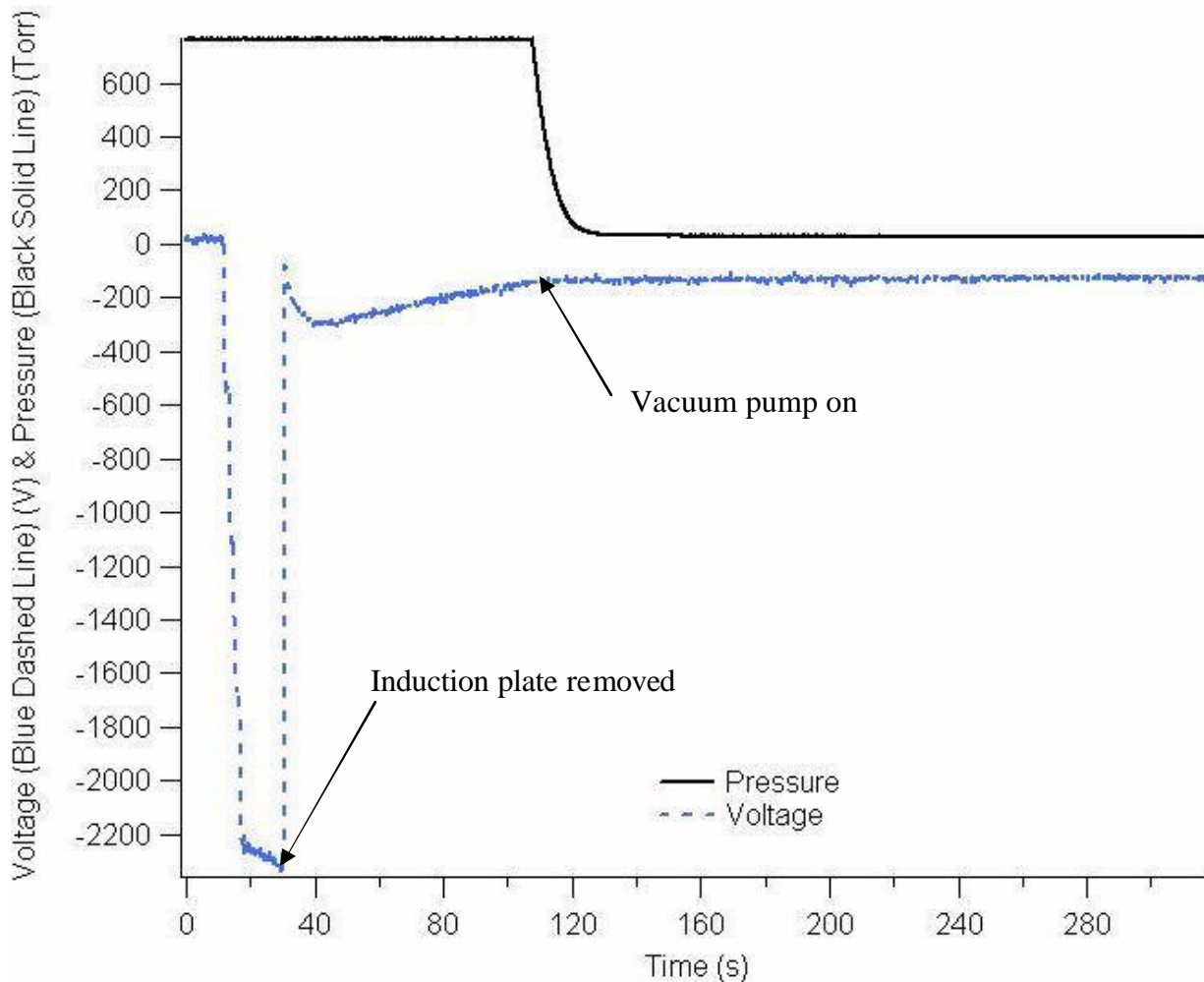


Fig. 18: Typical discharge for an inductively charged polymer sample (HDPE Sample #2) under lowered pressure. For comparison, the pressure decrease as a function of time is also shown.

Positive polarity induction experiments were also performed. The Keithley 247 was switched to provide approximately + 2000 V. The polymers were again exposed to the charged induction plate in no pump down baseline experiments and to lowered pressure experiments. Examples of the resultant data from these experiments are shown in Figs. 19 and 20, respectively. The results shown in Figs. 17 -20 are typical of all the other tested polymers (LDPE, PTFE, and polycarbonate). Only about 300 V of the approximately ± 2000 V remained on the samples after induction plate removal. No discontinuous discharges were noted in any of the induction charging experiments. This indicates that the source of the surface charge (in this case electrons) is not subject to evaporation caused by lowered pressure as are ions or charged molecules.

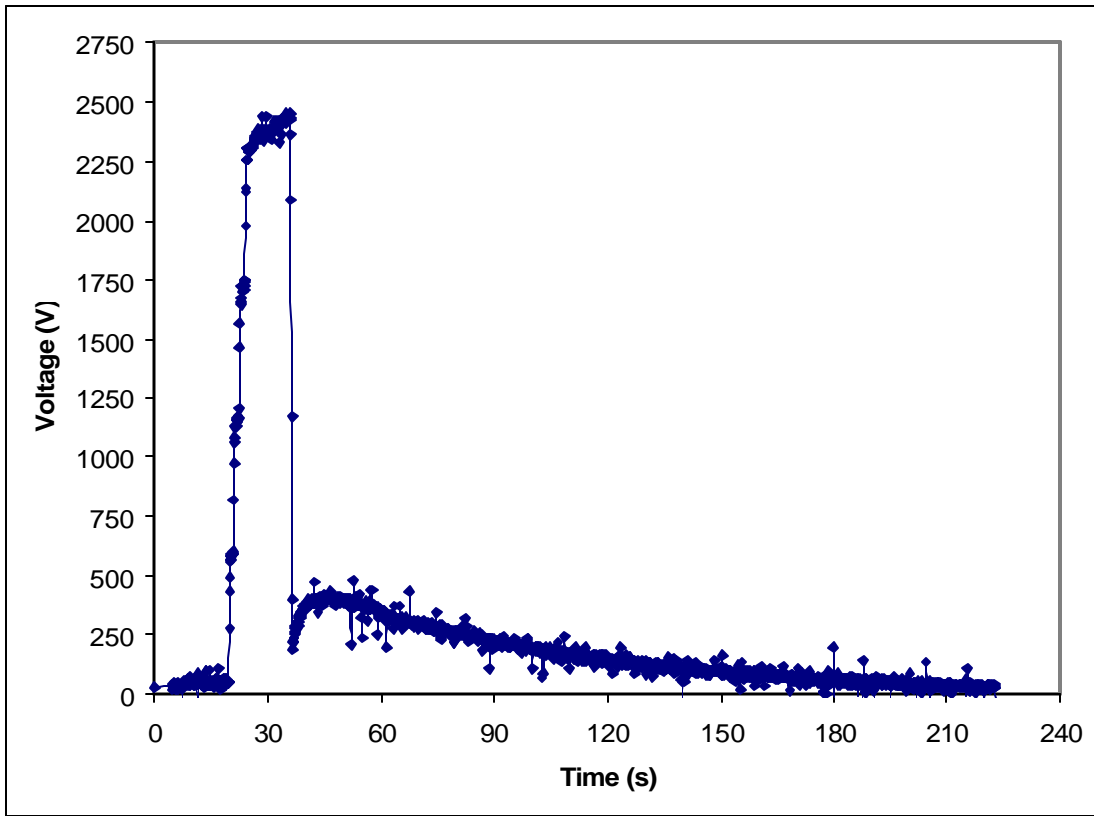


Fig. 19: HDPE sample # 1 positive polarity baseline induction experiment with no pump down.

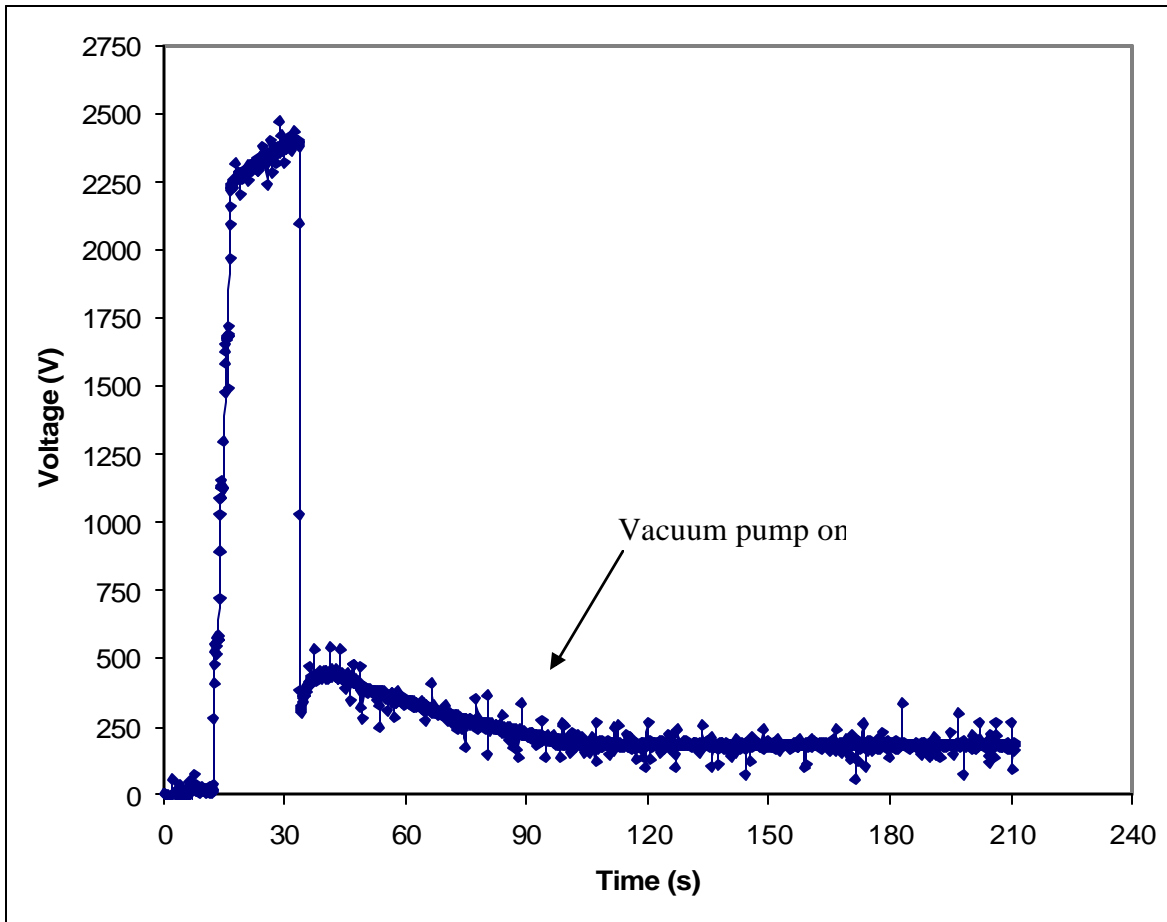


Fig. 20: HDPE sample # 2 positive polarity induction.

Part 3: Corona Experiments

Another way to place charge on a surface is to ionize air molecules and move them to the target surface electrostatically. This is accomplished by constructing a conducting plate with sharp, needle points to concentrate the electric field. The conducting plate is a thin sheet of brass penetrated by common steel needles. The plate and needles are supported by plastic hollow core poster board backing. The needles protrude from the insulating backing, shielding the polymer

sample from any field effects of the brass sheet. These needle points concentrate the electric field enough to ionize the air when about 3000 V dc is applied.

To move the ionized atoms and molecules to the target surface, a ground plate is placed behind the sample. The ionized particles will then move toward and adhere to the target surface. This corona charging apparatus is shown schematically in Fig. 21.

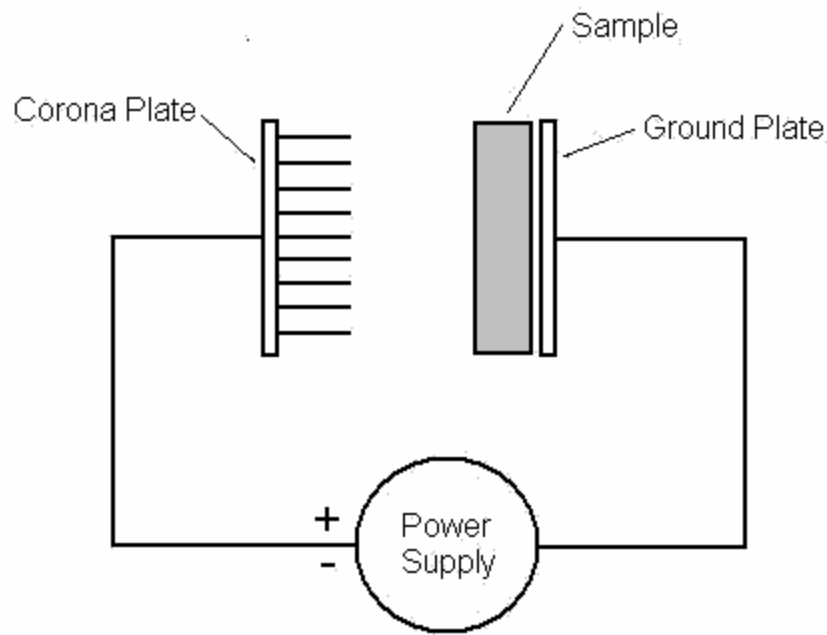


Fig. 21: Schematic of the corona charging experiment.

The triboelectric experimental apparatus was modified to allow placement of the corona plate near the polymer sample along with the ground plate. The corona plate is shown in Fig. 22.

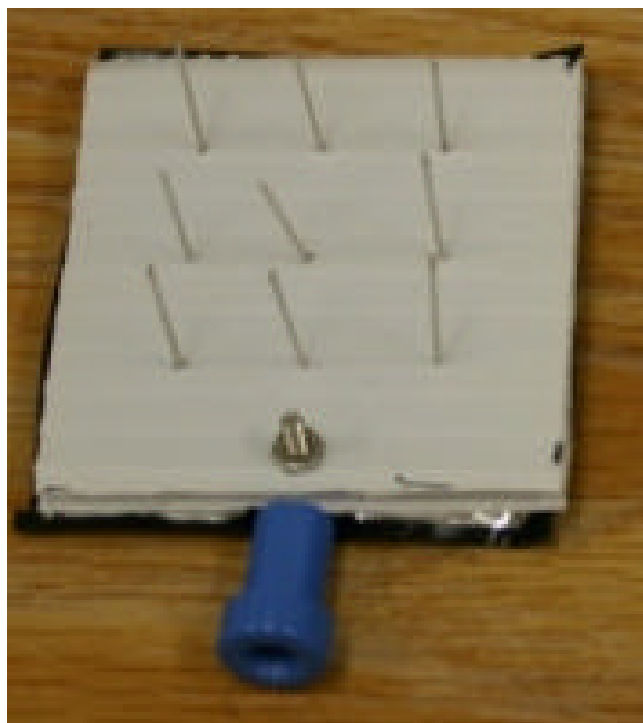


Fig. 22: Corona charge plate showing field points and electrical connector.

Four corona charging experiments were performed on each polymer. The corona charging voltage was set at approximately ± 3000 V. The corona plate was placed at approximately 1.0 cm away from the sample. The ground plate was placed in light, non-rubbing contact with the backside of the sample. Each sample was corona charged for approximately 60 seconds. The corona and ground plates were then removed, the chamber was sealed up and the vacuum pump started. It took approximately 1 minute to lower the chamber pressure. As in the triboelectric experiments, discontinuous discharges were observed for all polymers. Typical data for the corona experiments is shown in Fig. 23. If the vacuum pump was not turned on, there would be only a slow, diffusive discharge to the air as shown on the curve in Fig. 23 prior to the start of the vacuum pump at location 4.

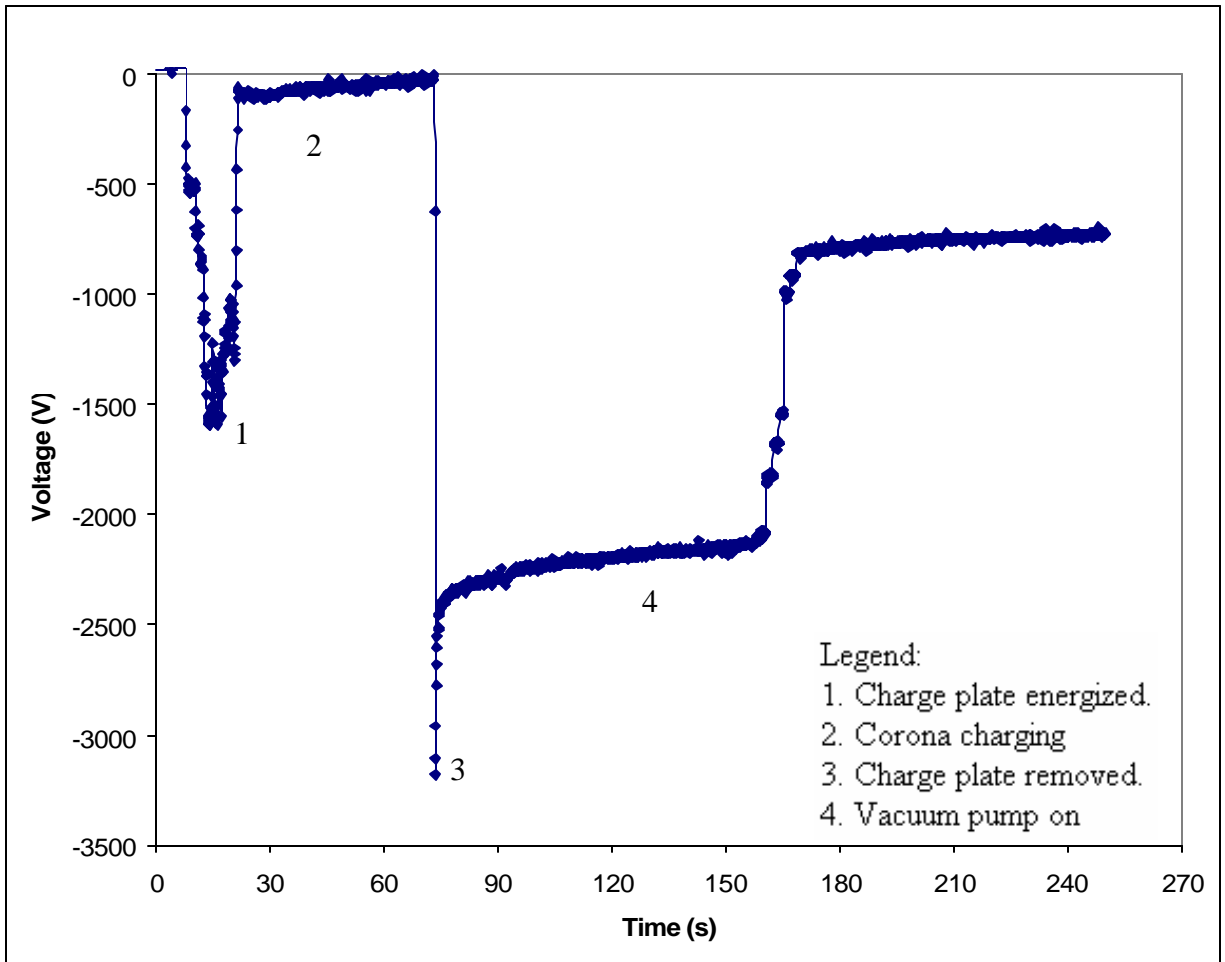


Figure 23: HDPE sample # 1 corona charging experiment.

Taking the corner points of the discharge data as before and curve fitting them to the model equation gives results for N and x_0 similar to those for triboelectric charging. An example of the curve fit for corona charging is given in Fig. 24. The corona charging curve fit data is summarized in Table 4.

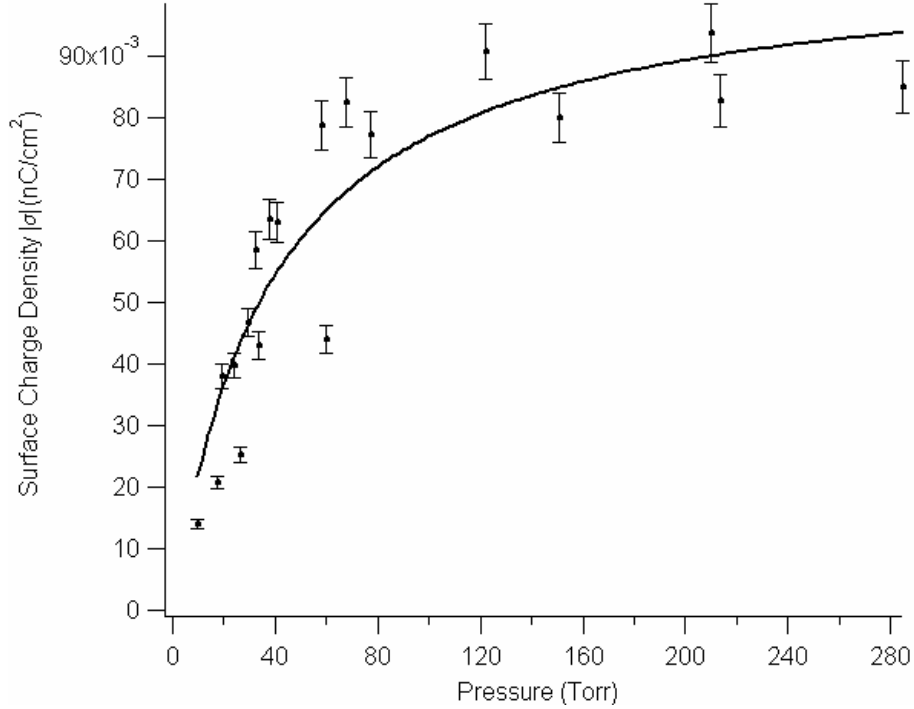


Figure 24: Corona charging data curve fit for PTFE.

Table 4

Curve fit values of polymer discharge data with the model equation for corona charging. Range values given are plus and minus one standard deviation.

Polymer	$N (\times 10^9)$	x_0 (eV)
HDPE (samples #1 – 3)	6.85 ± 1.55	-0.45 ± 0.01
LDPE (samples #1 – 3)	4.9 ± 2.35	$-0.46 \pm \begin{smallmatrix} 0.02 \\ 0.08 \end{smallmatrix}$
PTFE (samples #1 - 3)	4.69 ± 0.39	-0.47 ± 0.01
Polycarbonate (samples #1 - 3)	4.51 ± 0.57	-0.46 ± 0.01
PVC (samples #1 – 3)	7.7 ± 1.0	-0.45 ± 0.01
Styrene (samples #1 – 3)	7.0 ± 1.3	-0.45 ± 0.01
Nylon MD (samples #1 & 2)	2.34 ± 0.10	-0.53 ± 0.01
Nylon MD (sample #3, + V)	3.329 ± 0.085	-0.520 ± 0.003

Part 4: Metal – Insulator Triboelectric Experiments

In Chapter 2, extensive work by several researchers on metal – insulator triboelectric charging was noted. These works advocated the electron transfer model of metal – insulator triboelectric charging and introduced effective work functions for insulators similar in magnitude to those of metals (approximately 4 – 5 eV) [25, p. 12-84]. Yet none of these experiments varied atmospheric pressure after the separation of the two rubbing surfaces to determine the surface charge versus pressure characteristics of the system. As we have shown, lowering the pressure after triboelectric contact while measuring the surface charge can provide a clear indication of the nature of the charged species upon the surface.

For metal – insulator triboelectric experiments, three crystal oriented metals were selected. They are tungsten, W (111), nickel, Ni (111), and copper, Cu (111). These samples were selected because they all have the same crystal orientation which could expose any similarities or differences in triboelectric charging due to their crystal structure. Another reason for their selection is that nickel and copper are close together on the periodic table (regions VIIIA and IB) while tungsten is farther away (region VIA). The differences in electronic structure and work functions could also manifest themselves in triboelectric experimentation.

The metal samples are 1.0 centimeter in diameter and 1.0 mm thick. The samples were modified for attachment to the rubbing wheel of the triboelectric apparatus by adding Velcro[®] to one side. Since the metal samples were smaller in diameter than the rubbing wheel, many trial experiments were performed to insure that only the metal sample contacted the polymer and not the edges or any other part of the rubbing wheel. This experimental set-up is shown in Fig. 25.

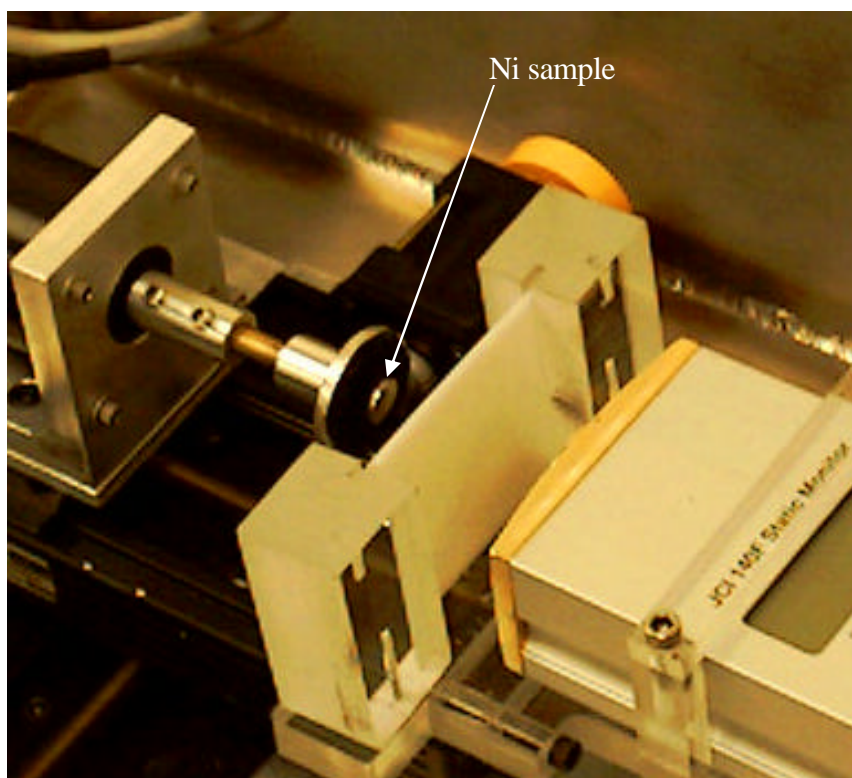


Fig. 25: Nickel sample attached to rubbing wheel in triboelectric apparatus.

Four polymers were selected for triboelectric experiments with the metal samples. They are HDPE, LDPE, PTFE, and polycarbonate. Samples # 8, 9, and 10 were selected from each of the polymers. Three experiments per metal and per polymer were performed. Also a baseline experiment was performed for each polymer where the pressure was not lowered. Each metal was cleaned with IPA both prior to and after each polymer type to reduce any cross-contamination from one polymer to the other. Also the polymer samples were cleaned with IPA both prior and after each series of metal experiments for the same reason. Two of the baseline experimental results are shown in Figs. 26 and 27.

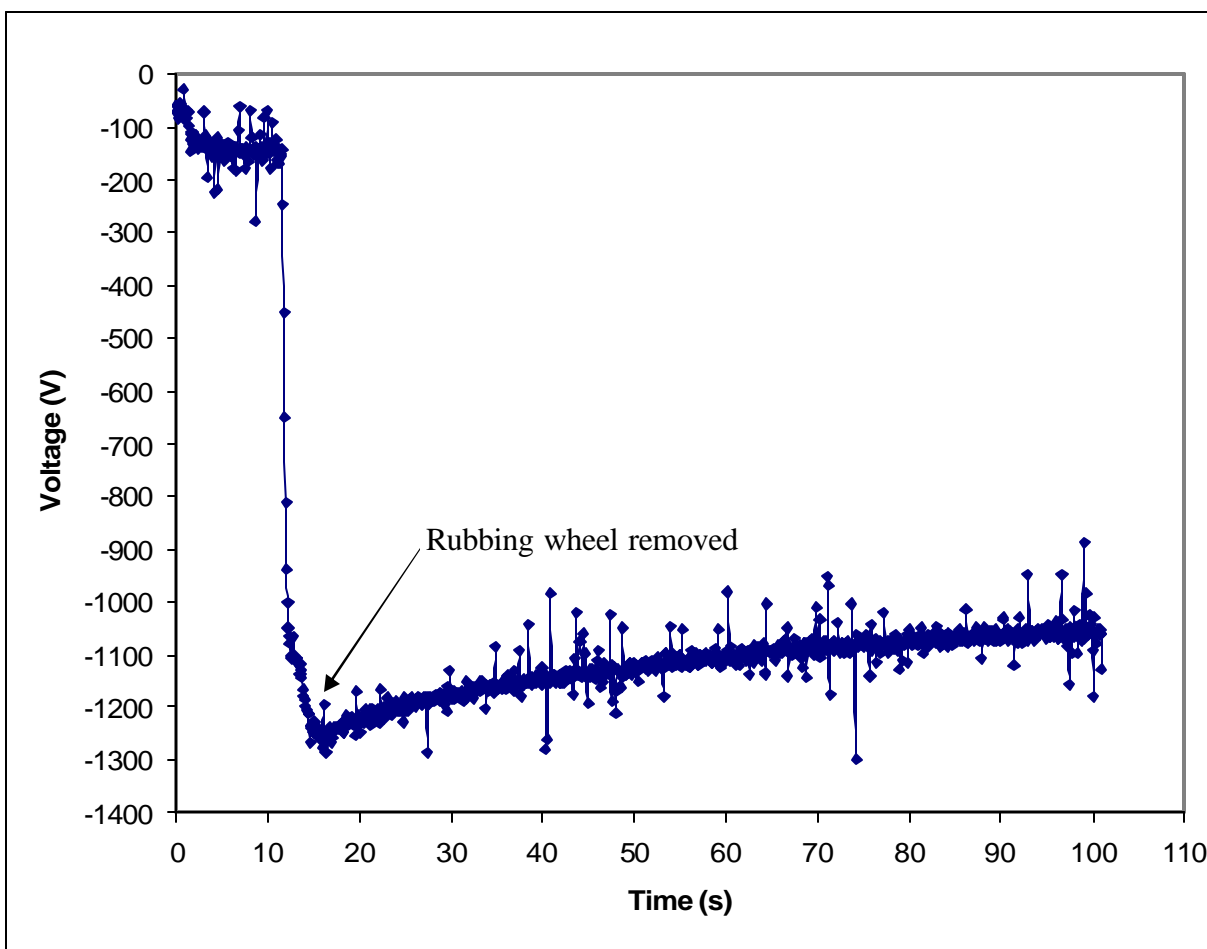


Fig. 26: PTFE sample # 8 tribocharging with Ni (111) baseline with no pressure reduction showing a slow, diffusive discharge with time.

All of the polymers used in the metal – insulator triboelectric experiments charged negative except for polycarbonate. Polycarbonate charged positive in the experiments for all three metals indicating that the metals are lower on the triboelectric series than polycarbonate. Since all the polymers were cleaned the same with IPA and handled carefully, the possibility of extraneous surface contaminants being the reason polycarbonate samples charged positive is very small.

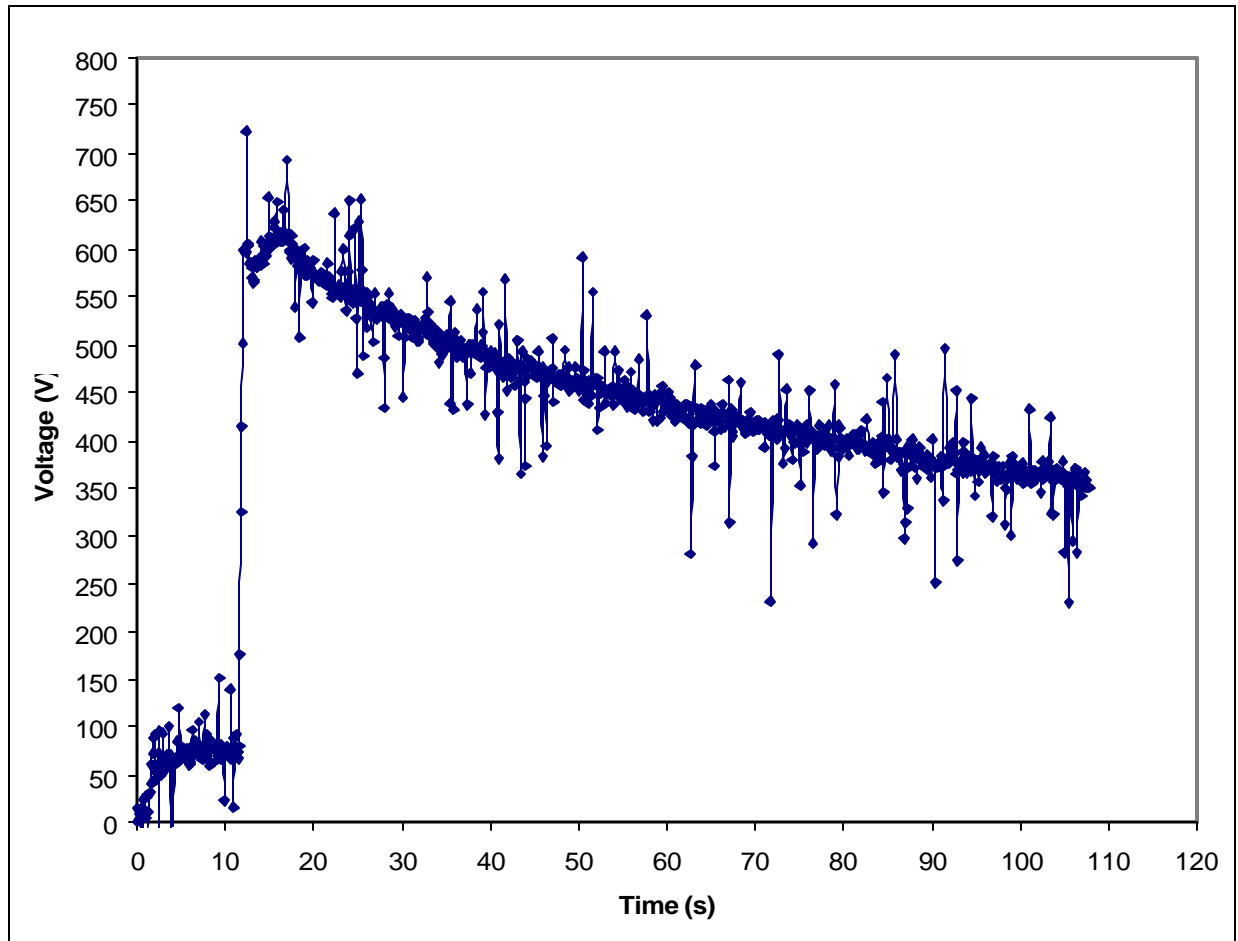


Fig. 27: Polycarbonate sample # 8 tribocharging with Cu (111) baseline with no pressure reduction showing a slow, diffusive charge decay in air.

The experiments with lowered pressure after metal – polymer separation produced discontinuous discharges, rapid continuous discharges, or both, similar to the insulator – insulator triboelectric and corona charging experiments. Examples of these pressure dependent discharges for metal – insulator tribocharging are given in Figs. 28 and 29. The similarity in pressure induced discharge between metal-insulator and insulator – insulator triboelectric charging indicates that the charge exchange mechanism is likely the same and that similar charged particles are leaving the surface.

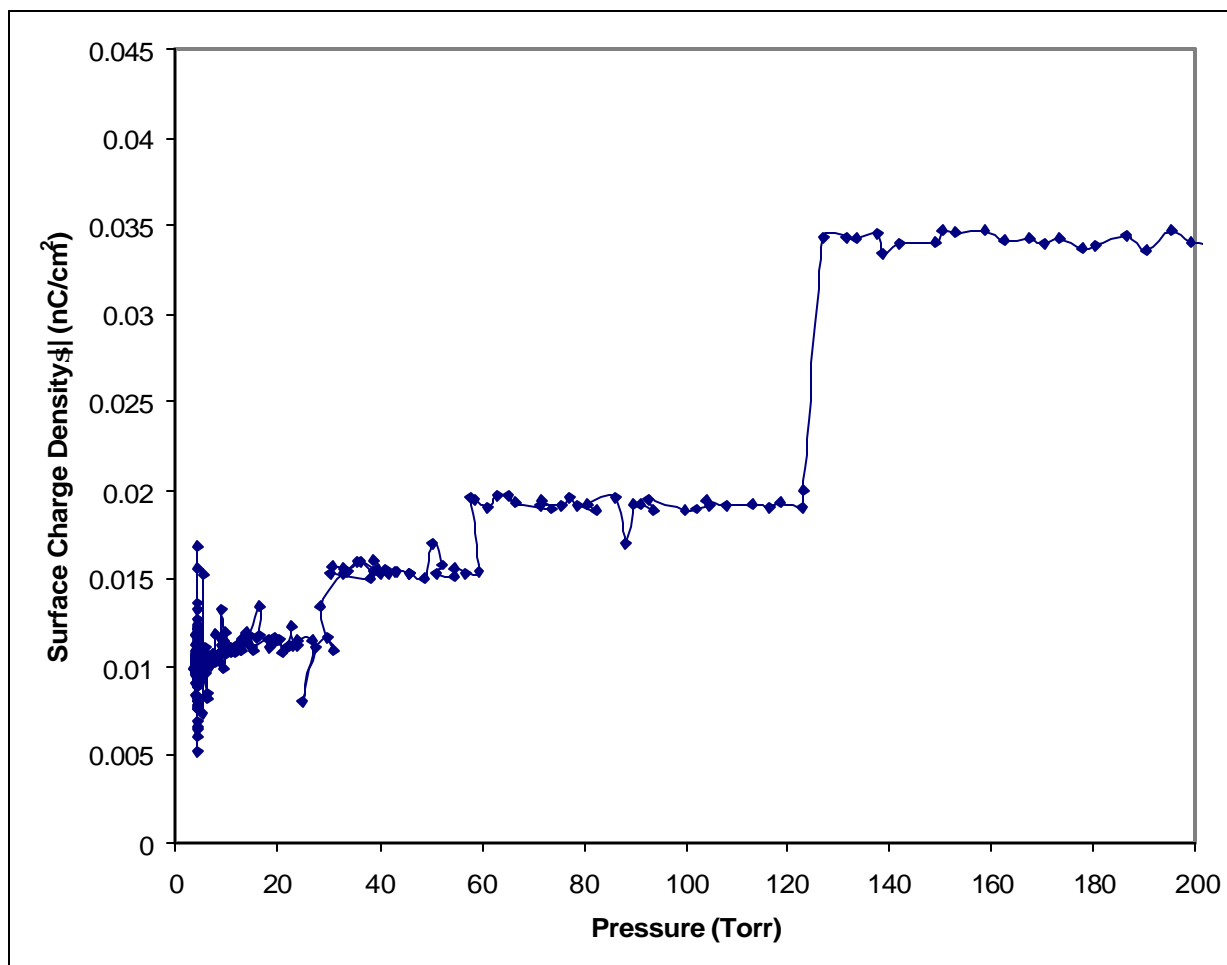


Fig. 28: Example of discontinuous discharge with lowered pressure for HDPE sample # 8 tribocharged with Ni (111).

The corner points of the discontinuous discharges on the data graphs and, where applicable, the points along continuous discharges were curve fit to the model equation. The resulting values of N and α_0 agree well with those obtained in the triboelectric and corona charging experiments. Examples of the curve fit plots are shown in Figs. 30 and 31. These fit values are summarized for all the polymers in Table 5. For some of the polymers, the curves varied from sample to sample as in Fig. 31. However, the difference in adsorption energy was

very small. This indicates that surface charging is dependent not only on material composition and number of adsorption sites but on sample history and morphology while x_0 varies little.

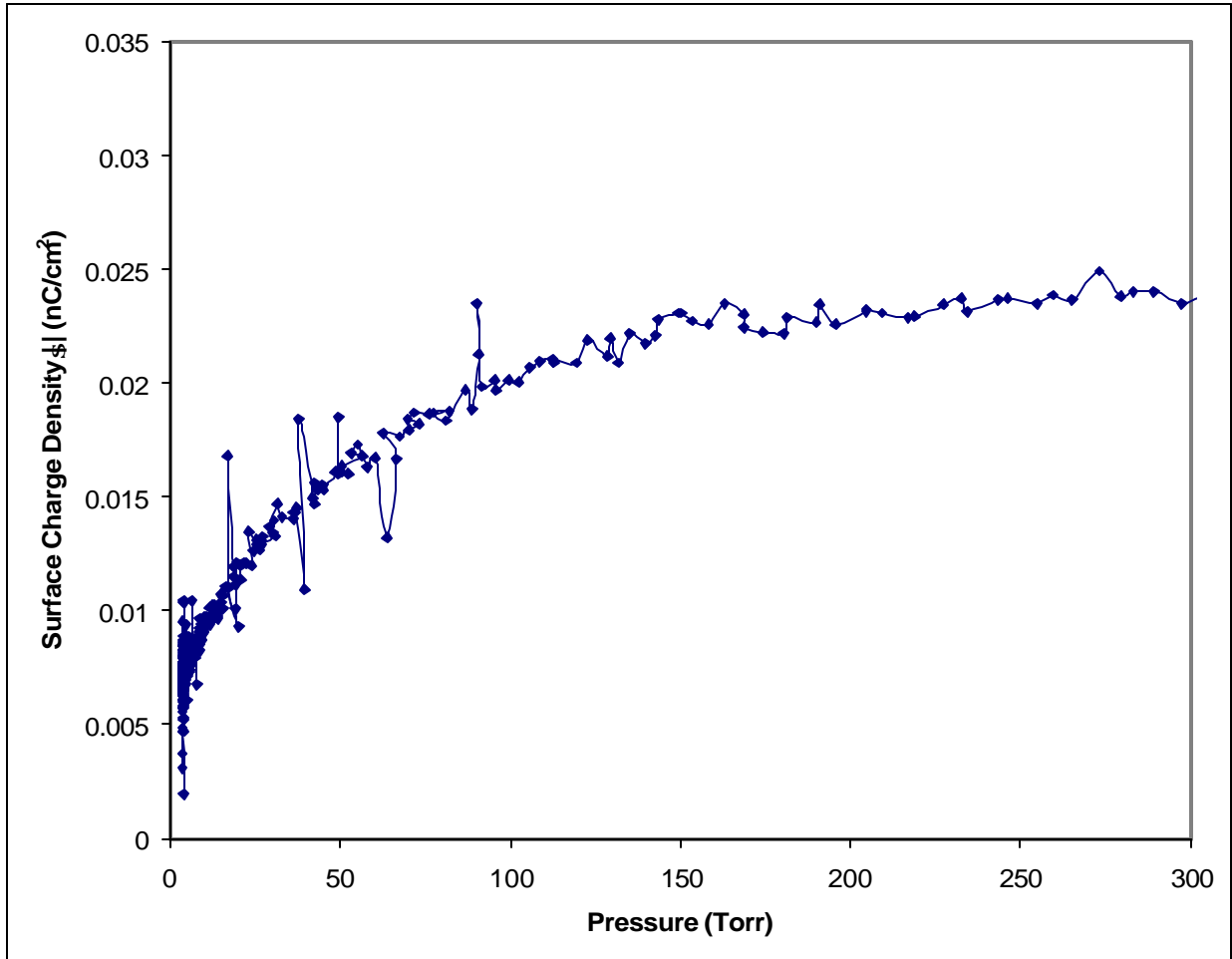


Fig. 29: Example of continuous discharge with lowered pressure for polycarbonate sample # 9 tribocharged with Cu (111).

The work functions of Ni (111), Cu (111), and W (111) used in the metal – insulator tribocharging experiments are 5.35 eV, 4.94 eV, and 4.47 eV, respectively [25, p. 12-84]. These values are one order of magnitude higher than the values of x_0 obtained in the curve fitting. Also

the effective electronic work functions that have been suggested for polycarbonate and PTFE are nearly the same, 4.26 ± 0.13 eV and 4.26 ± 0.05 , respectively [1, p. 29]. These values are also an order of magnitude larger than the values of x_0 for the polymers. This corroborates the hypothesis that the charged particles that left the surface because of lowered pressure were not electrons but weakly adsorbed ions. However, this data does not rule out some electron transfer taking place. More discussion on this will be presented in Ch. 5.

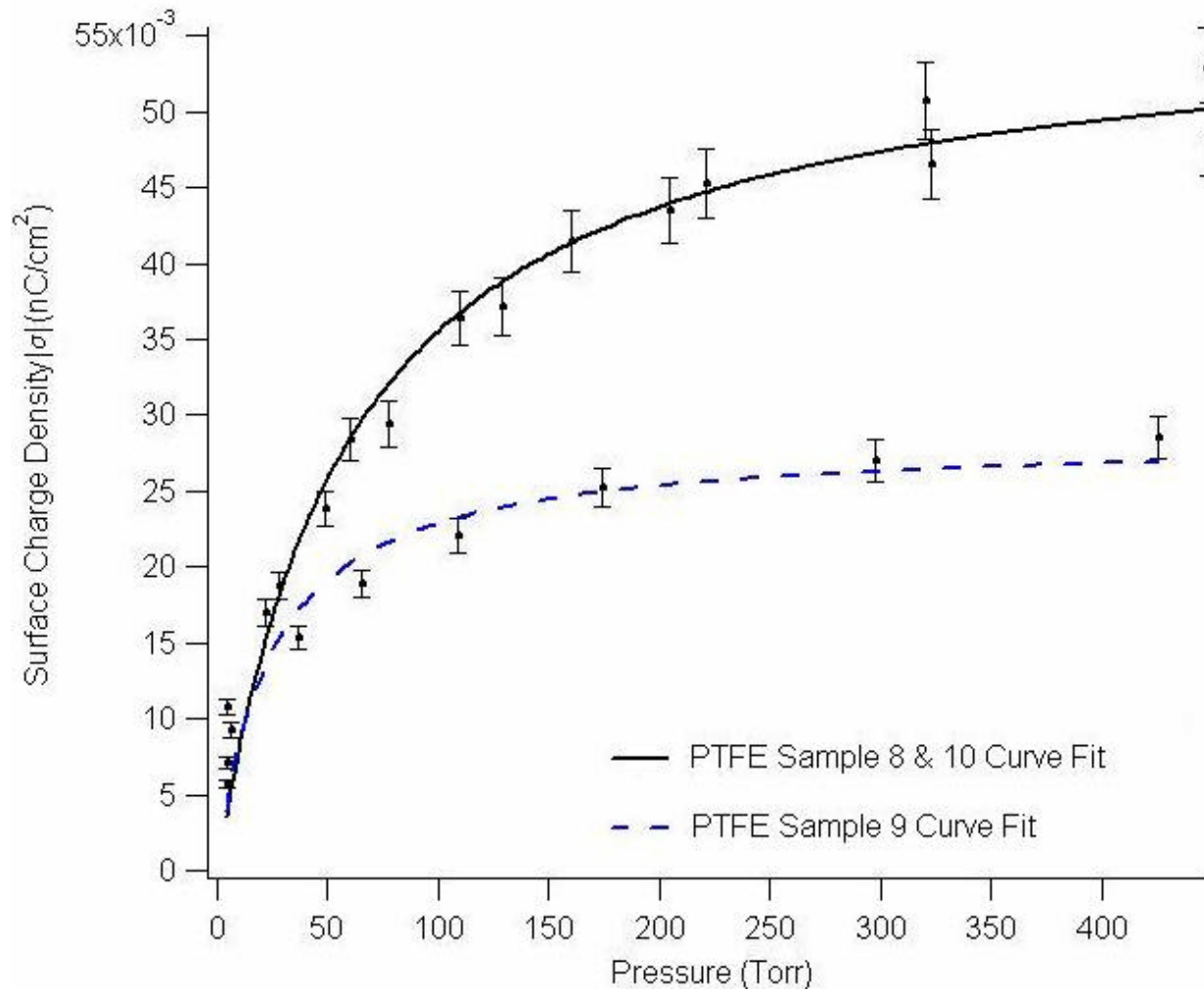


Fig. 30: Curve fit results for PTFE samples # 8, 9, and 10 tribocharged against Ni (111).

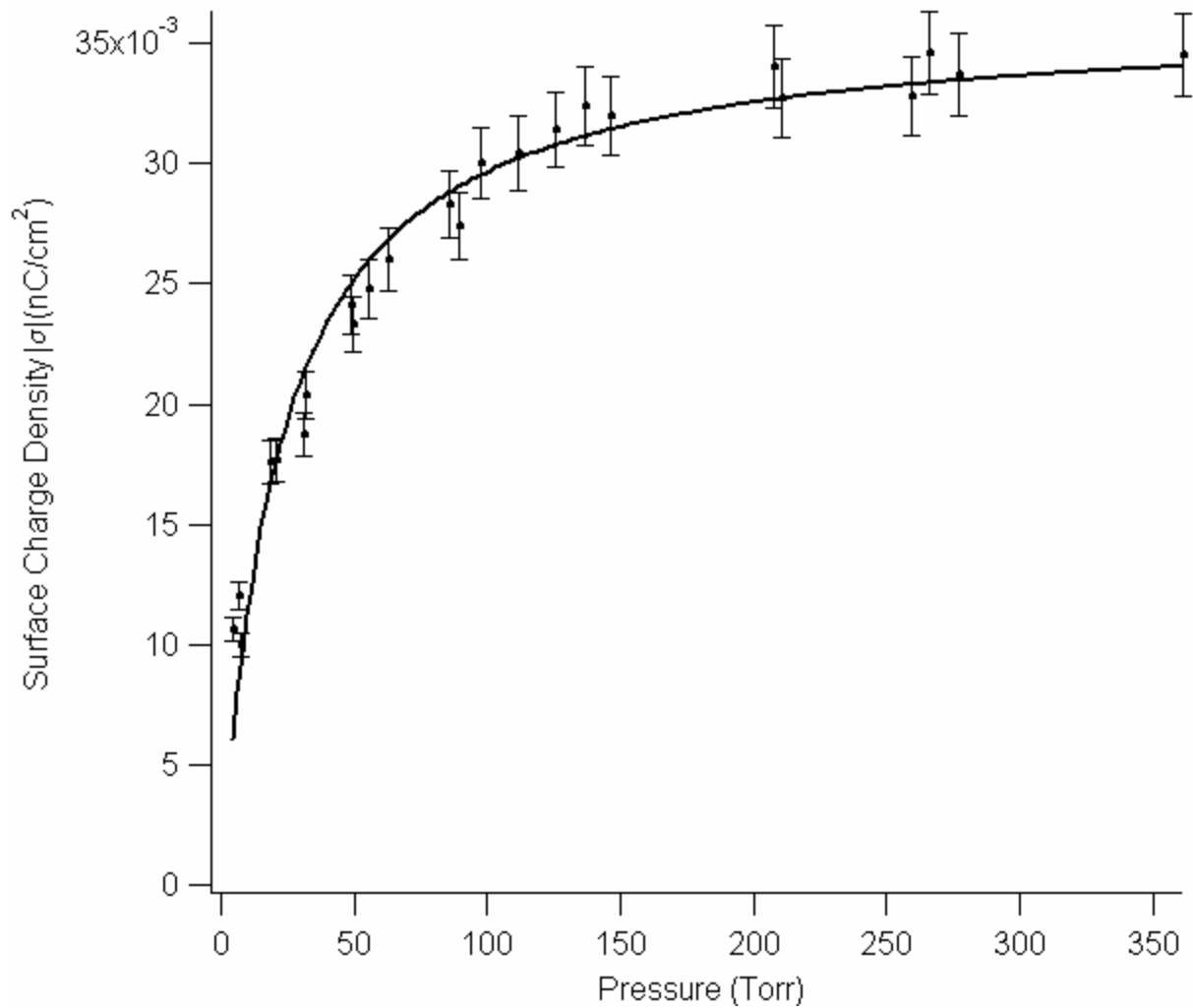


Fig. 31: Curve fit results for polycarbonate tribocharged with Ni (111).

Table 5

Curve fit values of polymer discharge data with the model equation for metal – insulator tribocharging. The range of values given is plus and minus one standard deviation.

Polymer	Metal	$N (\times 10^9)$	x_0 (eV)
HDPE	Cu (111)	3.0 ± 1.3	$-0.45 \pm \begin{smallmatrix} 0.01 \\ 0.03 \end{smallmatrix}$
HDPE	Ni (111)	2.21 ± 0.57	$-0.46 \pm \begin{smallmatrix} 0.01 \\ 0.03 \end{smallmatrix}$
HDPE	W (111)	0.84 ± 0.15	$-0.49 \pm \begin{smallmatrix} 0.01 \\ 0.03 \end{smallmatrix}$
LDPE	Cu (111)	0.556 ± 0.065	-0.51 ± 0.01
LDPE (samples #8 & 10)	Ni (111)	0.849 ± 0.066	-0.50 ± 0.01
LDPE (sample #9)	Ni (111)	0.425 ± 0.032	-0.53 ± 0.01
PTFE (samples #8 & 9)	Cu (111)	2.55 ± 0.12	$-0.460 \pm \begin{smallmatrix} 0.004 \\ 0.01 \end{smallmatrix}$
PTFE (sample #10)	Cu (111)	2.21 ± 0.15	-0.45 ± 0.01
PTFE (samples #8 & 10)	Ni (111)	2.51 ± 0.09	$-0.460 \pm \begin{smallmatrix} 0.003 \\ 0.004 \end{smallmatrix}$
PTFE (sample #9)	Ni (111)	1.26 ± 0.07	-0.48 ± 0.01
PTFE (samples #8 & 9)	W (111)	0.758 ± 0.057	-0.49 ± 0.01
PTFE (sample #10)	W (111)	1.126 ± 0.073	-0.48 ± 0.01
Polycarbonate (sample #8)	Cu (111)	1.8 ± 0.11	-0.48 ± 0.01
Polycarbonate (sample #9)	Cu (111)	1.07 ± 0.06	-0.49 ± 0.01
Polycarbonate (sample #11)	Cu (111)	2.137 ± 0.097	-0.470 ± 0.004
Polycarbonate	Ni (111)	1.592 ± 0.033	-0.490 ± 0.002
Polycarbonate (sample #8)	W (111)	0.468 ± 0.038	-0.49 ± 0.01
Polycarbonate (samples #9 & 11)	W (111)	0.912 ± 0.057	-0.48 ± 0.01

Part 5: Numerical Calculation of Ion Adsorption Energy

All the curve fit values for the adsorption energy, χ_0 , are consistent in magnitude over all triboelectric and corona charging experiments. To help determine whether the ~ -0.4 eV range of χ_0 obtained from curve fitting the experimental data is consistent with the physical chemistry of the surface and the adsorbed ions, numerical calculations of the adsorption energy of ions on polymer surfaces were performed at KSC by the Corrosion Technology Testbed [19A]. A software code called NWChem[®] [22], which can perform *ab initio* quantum mechanical electronic structure calculations as well as vibrational analysis, was used to calculate the adsorption energies of several ions on polymeric surfaces. For the adsorption energies, the geometries were first optimized using the Hartree-Fock self-consistent field method [27] which is an approximation to the electronic Schrödinger equation which can be solved numerically.

Numerical calculations of ion adsorption energies have been performed for HDPE and PTFE [19A]. HDPE was modeled as pentane, C₅H₁₂. PTFE was modeled as fluorine substituted pentane, C₅F₁₂. A five carbon chain was chosen as it was the minimum length that would allow the ions to interact with all the methylene (-CH₂) groups. Three ions were considered in these calculations, sodium (Na⁺), chlorine (Cl), and hydroxide (OH). Three stable adsorption configurations for HDPE and one for PTFE were found for the sodium ion. One stable configuration each for HDPE and PTFE were found for the chlorine ion. One stable configuration for the hydroxide ion was found for HDPE. These stable ion-polymer configurations are shown in Figs. 32 – 38.

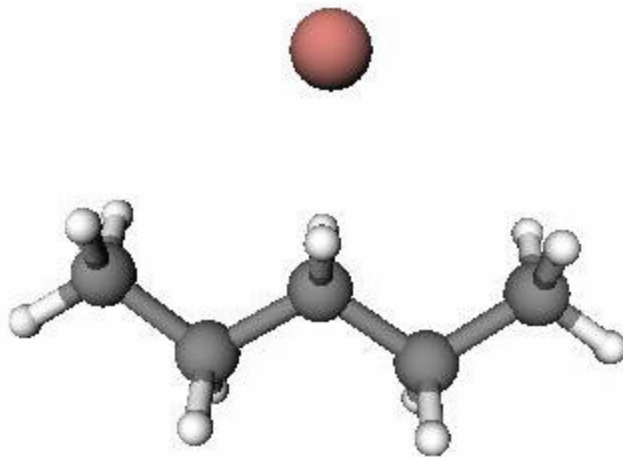


Fig. 32: Stable configuration A for a sodium ion adsorbed on HDPE modeled as C_5H_{12} .

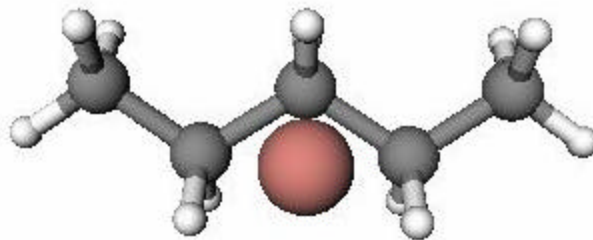


Fig. 33: Stable configuration B for a sodium ion adsorbed on HDPE modeled as C_5H_{12} .

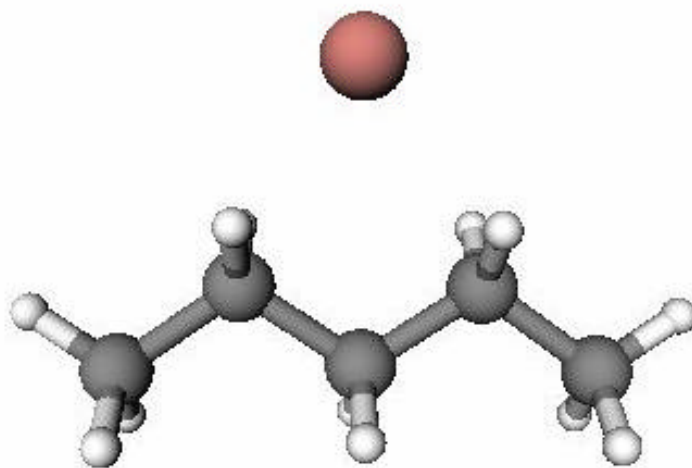


Fig. 34: Stable configuration C for a sodium ion adsorbed on HDPE modeled as C_5H_{12} .

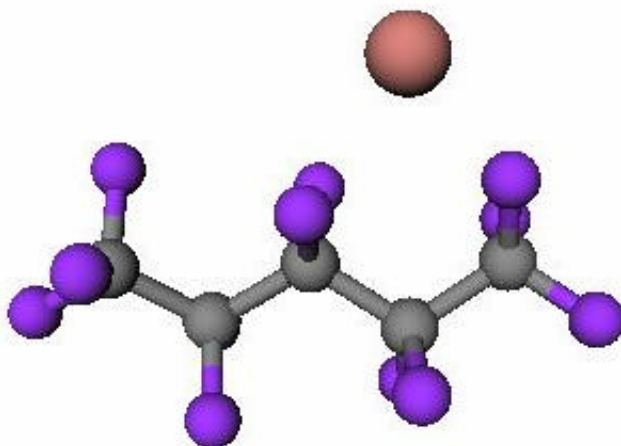


Fig. 35: Stable configuration for a sodium ion adsorbed on PTFE modeled as C_5F_{12} .

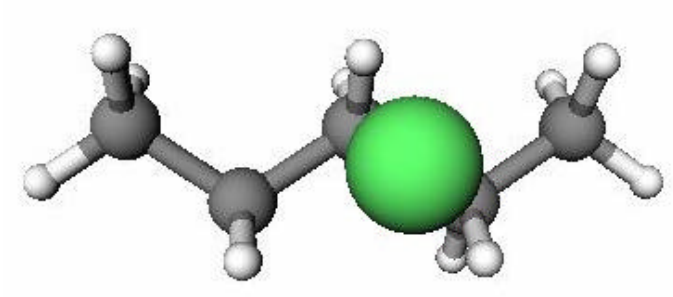


Fig. 36: Stable configuration for a chlorine ion adsorbed on HDPE modeled as C₅H₁₂.

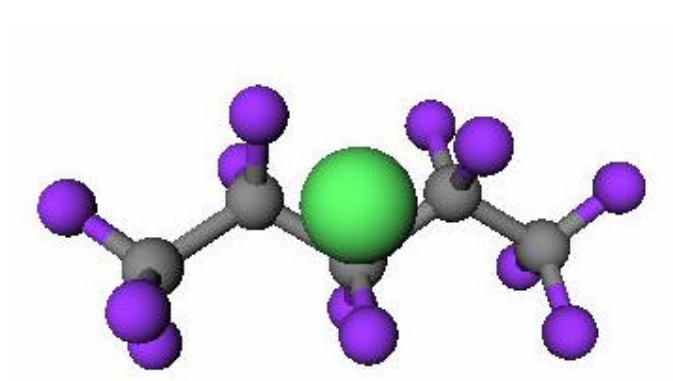


Fig. 37: Stable configuration for a chlorine ion adsorbed on PTFE modeled as C₅F₁₂.

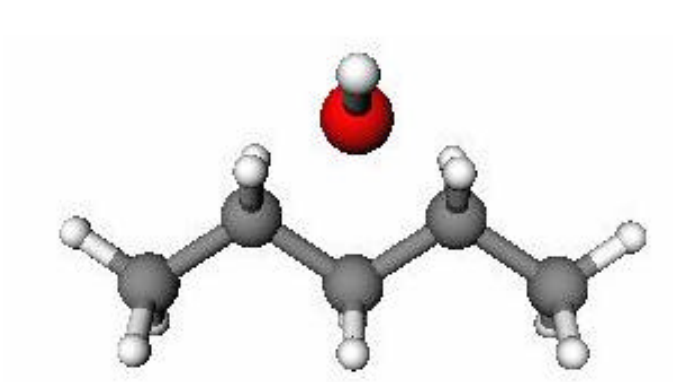


Fig. 38: Stable configuration for a hydroxide ion adsorbed on HDPE modeled as C₅H₁₂.

The adsorption energies calculated from these stable ion-polymer configurations are compared to the triboelectric data for wool and corona charging data in Table 6. The magnitudes of the calculated adsorption energies are mostly consistent with the curve fit values of \mathbf{x}_0 except for Chlorine, which is about one third the curve fit values for the wool triboelectric and corona experiments. We will return to the NWChem value for chlorine in Chapter 5.

Table 6
Comparison of numerical calculations of ion adsorption energies with curve fit values of ion adsorption energies. Range values given are plus and minus one standard deviation.

<u>Polymer/Ion</u>	<u>NWChem Result (eV)</u>	<u>Curve Fit Wool Tribo \mathbf{x}_0 (eV)</u>	<u>Corona Curve Fit \mathbf{x}_0 (eV)</u>
HDPE- Na^+ (A)	-0.4	$-0.470 \pm \begin{smallmatrix} 0.01 \\ 0.003 \end{smallmatrix}$	-0.45 ± 0.01
HDPE- Na^+ (B)	-0.38		
HDPE- Na^+ (C)	-0.47		
HDPE-Cl	-0.15		
HDPE-OH	-0.58		
PTFE- Na^+	-0.47	-0.44 ± 0.01	-0.47 ± 0.01
PTFE-Cl	-0.15		

CHAPTER FIVE: SUMMARY AND CONCLUSION

Insulator – insulator contact or triboelectric charging is the least physically understood of the three basic types of contact charging as far as the charge exchange mechanism is concerned. The charge exchange mechanism of the other two types of triboelectric charging, metal – metal and metal – insulator are, to various degrees better known. Many theories and experimental data have been put forward to explain insulator – insulator contact charging in terms of electron exchange only. These studies fail to address the fact that insulators do not have free or nearly free electrons to exchange upon physical contact and that other charged particles such as ions or charged molecules may play a more important role in triboelectric charging.

A fundamental knowledge of how insulators charge triboelectrically is of great importance in industry here on Earth. Much destruction, injury, and death occurs due to fires, explosions, or electrical failure caused by the electrostatic discharge from surfaces. In space, spacecraft can build up large voltages that can damage sensitive electronics and materials. On planetary surfaces, such as on the Moon or Mars there is fine dust that can electrostatically cling to spacecraft surfaces, space suits, movable joints, view ports, and solar cells causing the loss of function of these critical components. Also there are the beneficial uses of insulator triboelectrification in industry. An example is copy or facsimile machines which use electrostatics to apply a polymer based toner to the paper. Another example is the use of electrostatics to evenly apply coatings to surfaces. A fundamental understanding of the physical mechanism of insulator – insulator triboelectrification can lead to methods and processes to mitigate its hazards and to enhance its beneficial aspects.

In this research, the charge exchange mechanism for insulator – insulator triboelectric charging has been determined to be mostly ionic in nature. When polymer samples are charged by rubbing contact with wool or PTFE felt, the resulting discharge with lowered pressure shows that most of the surface charges are volatiles that evaporate off the surface in large masses or rapidly once their vapor pressure is reached. The discontinuous or stair-step discharges show that the thermodynamic equilibrium between the adsorbed surface ions and their gas phase counterparts is broken at what can be described as a critical build-up of perturbative forces. The corner points of the discharge data prior to the discharge were taken as quasi-equilibrium points and used in the curve fit calculations. In light of recent thinking on the matter, the corner points immediately after the discharge may be better quasi-equilibrium points since the system has just relaxed and is not yet experiencing a large build-up of perturbative forces. The use of the corner points after discharge should not significantly change the curve fit values of x_0 since it has been shown in Chapter 4 that various samples of the same polymer have different S versus P curves (such as Fig. 13) yet have similar curve fit values of x_0 .

The induction experiments charged the polymer samples by using a charged metal plate to add or remove electrons from the polymer surfaces. Upon lowered pressure, no discharge such as that for the triboelectric charging experiments was noted. Actually, the slow diffusive discharge in air experienced by the polymer samples as the electrons were neutralized by air ions was stopped upon lowering the pressure. That provided additional support to the idea that ions are involved in the triboelectric charging and discharging of insulator surfaces.

In the corona experiments, ions and charged molecules were placed on the polymer surface. A charged array of sharp needles was used to ionize the air. These air ions and charged molecules were then drawn electrostatically to the target polymer surface by a metal ground plate

placed behind the polymer. Discontinuous and/or rapid discharge with lowered pressure was found to be similar to that obtained when the polymer samples were charged triboelectrically. The curve fit values of the total number of occupiable surface sites, N , and the surface adsorption energy, χ_0 , from both the triboelectric and corona experiments have the same range (approximately -0.4 eV), giving strong evidence that ions are responsible for the discharges noted in the triboelectric experiments. The values of χ_0 for the triboelectric experiments and the corona experiments are compared in Table 7. The adsorption energies from all three experiment regimes agree well.

Table 7
Comparison of curve fit values of the adsorption energies from the triboelectric and corona experiments. Range values given are plus and minus one standard deviation.

Polymer	Curve Fit χ_0 (eV)		
	Wool Tribo	PTFE Felt Tribo	Corona
HDPE	$-0.470 \pm \begin{smallmatrix} 0.01 \\ 0.003 \end{smallmatrix}$	-0.46 ± 0.01	-0.45 ± 0.01
LDPE	-0.48 ± 0.01	-0.49 ± 0.01	$-0.46 \pm \begin{smallmatrix} 0.02 \\ 0.08 \end{smallmatrix}$
PTFE	-0.44 ± 0.01	-0.46 ± 0.01	-0.47 ± 0.01
Polycarbonate	$-0.46 \pm \begin{smallmatrix} 0.01 \\ 0.02 \end{smallmatrix}$	-0.46 ± 0.01	-0.46 ± 0.01

Metal – insulator triboelectric experiments were performed to determine if there could be electron exchange between the contacting metal and insulator as reported by other researchers. The discharge observed from these experiments showed the same discontinuous or rapid

continuous curves as in the triboelectric or corona charging experiments. Curve fit values of χ_0 agree well with the curve fit values from the other experiments. This shows that metal – insulator contact charging in air at room temperature (~ 300 K) is mostly the exchange of surface ions also.

To determine whether or not these curve fit values of χ_0 have physical reality, a quantum mechanical numerical calculation was performed. Two polymers, HDPE and PTFE were modeled and three ions, Na^+ , Cl^- , and OH^- were used. Except for Cl^- , which had a calculated adsorption energy about one third of the curve fit value, the binding or adsorption energy values resulting from these calculations agree well with the curve fit values for χ_0 . This agreement between adsorption energy values shows that surface adsorbed ions can be responsible for the discharges observed. Since more than one charged species can be on a surface, the curve fit values of χ_0 could very well be averages of their adsorption energies. Averaging the calculated adsorption energies of Cl^- and OH^- adsorbed on HDPE gives a value of -0.365 eV which is closer to the curve fit value of χ_0 (-0.47 eV, wool tribocharging).

None of the surface charge density curves went to zero under reduced pressure. In some experiments, as much as 20% of the initial charge remained on the polymer surface after pump down of the chamber. There could be one of two explanations for this remaining charge.

One, the residual charge is caused by ions or charged molecules that have a lower vapor pressure than the vacuum chamber could achieve (~ 4 Torr). This is not unreasonable since the remaining layers of charge would be very close to the electric double layer at the substrate surface where the Gouy-Chapman potential [12] is very strong.

Two, while the majority of charge exchange between insulators and metals/insulators has been shown to be due to ion exchange, there is some electron exchange between the two

surfaces. As seen in the induction experiments, electronic surface charge is not efficiently removed by lowering the pressure and that could explain the residual charge. Further experiments with much better vacuum systems will be required to determine which of these two explanations for the residual surface charge is correct.

Data such as those presented in Fig. 7 indicate that discharge in most samples has a marked non-equilibrium behavior, despite the fact that the pressure was decreased relatively slowly with respect to the intrinsic dynamical scales of the ions on the solvent. One notices that the voltage (or charge) in some samples does not follow exactly the quasi-equilibrium curve predicted by Eq. (3). Every now and then the charge tends to level and saturate, becoming nearly insensitive to the external pressure. We speculate that during these time intervals, some unusually stable configuration of adsorbed charges is reached, providing some local (but not global) minimum to the free energy. However, upon driving the pressure further down, a critical point is reached when the charge configuration at the surface becomes unstable and a large discharge, similar to an avalanche, ensues until a new equilibrium point is found.

This effect has some resemblance to other processes in nature where time evolution is driven by a combination of internal dynamics due to cohesive forces and external driving, resulting in “avalanches”. For instance, this is the case for earthquakes, sand piles, and the stock market. It has been proposed that the unifying principal among the time evolution of these diverse systems is self-organized criticality, namely, the capability of a complex, interacting system with many degrees of freedom to live in a critical state [28]. Such systems have the intrinsic capability of correcting for deficits or excesses, independently of any control parameter. For instance, upon dropping sand over a pile, a series of random avalanches, large and small, occur, making the pile slope independent of the rate at which sand is dropped.

One way to characterize self-organized behavior is to find out how the size, duration, and interval of avalanches are distributed. Critical systems should show power-law (scale free) distributions. Unfortunately, the data collected during the triboelectric discharge experiments are insufficient for an accurate analysis.

Future triboelectric experiments could probe different aspects that have not yet been studied. Among these are: different gases, higher than atmospheric pressure, varying temperature, and changing the surface ion/contaminant concentrations.

Different gases, such as GN_2 , GHe , and CO_2 , could possibly allow for the adsorption and subsequent desorption of different ion species than air. The experiments described in this work dealt with air at a pressure range from atmospheric (760 Torr) to about 4 Torr. Near atmospheric pressure, the S versus P curve approaches a saturation level where you would expect all the adsorption sites, to be filled. Is there a saturated plateau above atmospheric pressure or is this a function of both pressure and temperature? Temperature is a significant term in the model equation appearing in the denominator. Varying the temperature should vary the adsorption and desorption rates accordingly causing changes in curve fit values of N and x_0 . Surface ion concentration can be changed by immersing the sample in various solutions of known molarity such as solutions of water with solvated NaCl or KCl .

**APPENDIX A: DERIVATION OF THE TWO-PHASE EQUILIBRIUM
MODEL WITH EFFECTIVE ELECTROSTATIC POTENTIAL**

- **Gas Phase**

The Hamiltonian of a gas of charged particles interacting electrostatically with the adsorbed ions via a surface potential of the Gouy-Chapman type [12] is given by the sum of kinetic and electrostatic potential energies. The Hamiltonian can be written as

$$H = \sum_{i=1}^N \left(\frac{p_i^2}{2m} + V_0 e^{-kz} \right), \quad (\text{A1})$$

where p is the particle's momentum, m is its mass, k is the inverse Debye length or screening length which is dependent on charged particle concentration, and z is the distance from the surface. Equation (A1) amounts to an approximation to the many-particle interacting problem. When direct interparticle interactions are neglected, the total Hamiltonian is the sum of independent terms, each one corresponding to a single particle. The effect of the Coulomb interactions is taken into account in a phenomenological or effective manner by assuming that each particle sees a modified attractive potential towards $z = 0$ (the surface). The partition function for a single particle is given by

$$z(1, T) = \frac{1}{h^3} \int_{\forall} \int_{-\infty}^{\infty} e^{-H/k_B T} d^3 p d^3 r. \quad (\text{A2})$$

where \forall is the volume, k_B is Boltzmann's constant, and T is the temperature. Substituting in equation (A1) we get

$$z(1, T) = \frac{1}{h^3} \int_0^{z_0} \int_0^{y_0} \int_0^{x_0} \int_0^{\infty} \int_0^{\infty} \int_0^{\infty} \exp \left[- \left(\frac{p_x^2 + p_y^2 + p_z^2}{2m} + V_0 e^{-kz} \right) \frac{1}{k_B T} \right] dp_x dp_y dp_z dx dy dz. \quad (\text{A3})$$

Performing the integrals over momentum space and the x and y coordinates gives

$$z(1, T) = \frac{(2\mathbf{p} m k_B T)^{3/2}}{h^3} x_0 y_0 \int_0^{z_0} \exp(-V_0 e^{-kz}) dz. \quad (\text{A4})$$

Making the substitution

$$\frac{(2\mathbf{p})^{3/2}}{h^3} = \left(\frac{2\mathbf{p}}{h^2}\right)^{3/2} = \left(\frac{2\mathbf{p}}{h^2} \frac{2\mathbf{p}}{2\mathbf{p}}\right) = \left(\frac{1}{2\mathbf{p}\hbar^2}\right)^{3/2}$$

gives

$$z(1, T) = \left(\frac{m k_B T}{2\mathbf{p}\hbar^2}\right)^{3/2} x_0 y_0 \int_0^{z_0} \exp(-V_0 e^{-kz}) dz. \quad (\text{A6})$$

Now we can define the thermal wavelength as

$$\mathbf{l} = \left(\frac{m k_B T}{2\mathbf{p}\hbar^2}\right)^{-1/2}. \quad (\text{A7})$$

Using Eq. (A7) in Eq. (A6) gives

$$z(1, T) = \frac{x_0 y_0 z_0}{\mathbf{l}^3} \int_0^{z_0} \exp(-V_0 e^{-kz}) dz. \quad (\text{A8})$$

Equation (A8) is analytically intractable. A way to circumvent this difficulty is to make variable changes to transform the integral into an analytic form. The first variable change is $z = uz_0$. This gives

$$z(1, T) = \frac{x_0 y_0 z_0}{\mathbf{l}^3} \int_0^1 \exp\left(-\frac{V_0}{k_B T} e^{-kz_0 u}\right) du. \quad (\text{A9})$$

We define the volume as the length and width of the sample and a distance z_0 from the surface or $\mathbf{v} = x_0 y_0 z_0$. The next substitution is $u = \mathbf{l}/v$. This gives

$$z(1, T) = \frac{\mathbf{v}}{\mathbf{l}^3} \int_1^\infty \exp\left(-\frac{V_0}{k_B T} e^{-kz_0/\mathbf{v}}\right) \frac{d\mathbf{v}}{\mathbf{v}^2}. \quad (\text{A10})$$

For high concentrations, $\exp(-kz_0/v) \sim 1$. Making this substitution into Eq. (A10) gives

$$z(1, T) \cong \frac{\mathcal{V}}{I^3} e^{-V_0/k_B T} \int_1^\infty \frac{dv}{v^2}. \quad (\text{A11})$$

The integral in Eq. (A11) can be solved analytically and has a value of 1. For N particles we can write Eq. (A11) as

$$z(N, T) = \frac{1}{N!} [z(1, T)]^N. \quad (\text{A12})$$

To get to the gas phase chemical potential, we need to use the grand partition function [20].

$$Z_G = \sum \frac{1}{N!} [z(1, T) \exp(\mathbf{m}_g/k_B T)]^N, \quad (\text{A13})$$

where \mathbf{m}_g is the gas phase chemical potential. Using the series expansion for e^x , we can write Eq. (A13) as

$$Z_G = \exp \left[\frac{\mathcal{V}}{I^3} \exp \left(\frac{-V_0}{k_B T} \right) \exp \left(\frac{\mathbf{m}_g}{k_B T} \right) \right]. \quad (\text{A14})$$

The grand potential energy is given by

$$\Omega_G = -k_B T \ln Z_G = -k_B T \frac{\mathcal{V}}{I^3} \exp \left(\frac{-V_0}{k_B T} \right) \exp \left(\frac{\mathbf{m}_g}{k_B T} \right). \quad (\text{A15})$$

Pressure can be found by taking the partial derivative of the grand potential energy with respect to volume keeping the chemical potential and temperature constant.

$$P = - \left(\frac{\partial \Omega_g}{\partial \mathcal{V}} \right)_{\mathbf{m}_g, T} = \frac{k_B T}{I^3} \exp \left(\frac{-V_0}{k_B T} \right) \exp \left(\frac{\mathbf{m}_g}{k_B T} \right). \quad (\text{A16})$$

Solving Eq. (A16) for the chemical potential gives

$$\mathbf{m}_g = k_B T \ln \left[\frac{\mathbf{l}^3}{k_B T} \frac{P}{\exp\left(\frac{-V_0}{k_B T}\right)} \right]. \quad (\text{A17})$$

The second term in the logarithm of Eq. (A17) can be viewed as the effective pressure due to the addition of electrostatic forces.

- **Adsorbed Surface Phase**

The total Hamiltonian of adsorbed surface particles can be written as

$$H = -n\mathbf{x}_0. \quad (\text{A18})$$

Here n is the number of occupied surface sites and \mathbf{x}_0 is the adsorption energy. The partition function is given by

$$z(n, T) = \binom{N}{n} \exp\left(-H/k_B T\right) = \frac{N!}{(N-n)!n!} \exp\left(-H/k_B T\right), \quad (\text{A19})$$

where N is the total number of occupiable surface sites. The grand partition function is the sum over all particles and is given by

$$Z_G = \sum_{n=0}^N \frac{N!}{(N-n)!n!} \exp\left[n\left(\frac{\mathbf{x}_0 + \mathbf{m}_s}{k_B T}\right)\right], \quad (\text{A20})$$

where μ_s is the surface chemical potential. By expanding Eq. (A20), we get a binomial series that can be written in a finite form by

$$Z_G = \left[1 + \exp\left(\frac{\mathbf{x}_0 + \mathbf{m}_s}{k_B T}\right) \right]^N. \quad (\text{A21})$$

The grand potential energy is found as before.

$$\Omega_G = -k_B T \ln \left\{ \left[1 + \exp \left(\frac{\mathbf{x}_0 + \mathbf{m}_s}{k_B T} \right) \right]^N \right\} = -k_B T N \ln \left[1 + \exp \left(\frac{\mathbf{x}_0 + \mathbf{m}_s}{k_B T} \right) \right]. \quad (\text{A22})$$

The number of occupied sites, n , can be found by taking the partial derivative of the grand potential energy with respect to the chemical potential keeping temperature constant.

$$n = - \left(\frac{\partial \Omega_G}{\partial \mathbf{m}_s} \right)_T = N \frac{1}{1 + \exp \left(\frac{(\mathbf{m}_s + \mathbf{x}_0)}{k_B T} \right)}. \quad (\text{A23})$$

Solving Eq. (A23) for the chemical potential gives

$$\mathbf{m}_s = -k_B T \ln \left(\frac{N}{n} - 1 \right) - \mathbf{x}_0. \quad (\text{A24})$$

- **Equilibrium**

The condition for equilibrium between a gas phase and an adsorbed surface phase is the equality of the respective chemical potentials. Setting Eqs. (A17) and (A24) equal and solving for n gives

$$n = N \frac{1}{\left(\frac{k_B T}{I^3} \right) \left(\frac{\exp \left(\frac{-V_0}{k_B T} \right)}{P} \right) \exp \left(\frac{-\mathbf{x}_0}{k_B T} \right) + 1}. \quad (\text{A25})$$

- **Surface Charge Density**

The total enclosed charge, Q , on a surface, can be expressed in terms of electric field, E , and the surface area, A , using Gauss's law. Assuming single ionization, Gauss's law can be written in terms of the number of occupied surface sites.

$$Q = \epsilon_0 EA = \mathbf{s}A = nq_e, \quad (\text{A26})$$

where \mathbf{s} is the surface charge density. Solving Eq. (A26) for n , substituting it into equation (A25), and solving the resulting equation for \mathbf{s} gives

$$\mathbf{s} = q_e \frac{N}{A} \frac{1}{\left(\frac{k_B T}{I^3} \right) \left(\frac{\exp\left(-V_0/k_B T\right)}{P} \right) \exp\left(-x_0/k_B T\right) + 1} \quad (\text{A27})$$

which is Eq. (2) in chapter 3.

- **Estimation of the Surface Potential Energy, V_0**

The numerical values of the inverse Debye length, \mathbf{k} , and the surface potential energy, V_0 , were evaluated in the following way. In MKS units the inverse Debye length is defined by

$$\mathbf{k} = \sqrt{\frac{q_e^2}{\epsilon \epsilon_0 k_B T} n_{ion}} \quad (\text{A28})$$

Where $q_e = 1.602 \times 10^{-19}$ C is the electron charge, $\epsilon_0 = 8.854 \times 10^{-12}$ F·m⁻¹ is the vacuum permittivity, $\epsilon \sim 10$ is the surface water layer dielectric function, and n_{ion} is the number density of ions solvated in the water layer. We have used the sodium concentration provided by the Cocoa city public works web site to estimate n_{ion} [29]. This was done because KSC uses Cocoa water and the ion content of the water the experimental samples were exposed to should be similar to that measured by the city. The value given for the sodium concentration is 77 ppm. Converting this to density gives 0.077 kg·m⁻³. The mass of the sodium (Na⁺) ion is 3.82×10^{-26} kg. Dividing this into the density gives $n_{ion} = 2.02 \times 10^{24}$ m⁻³. The inverse Debye length is calculated from Eq. (A28) to be $\mathbf{k} = 3.8 \times$

10^8 m^{-1} . This value corresponds to a screening length of about 2.6 nm. Thus ions at this concentration are very effective in screening the charge adsorbed on the insulator surface.

The dimensionless ratio between the surface potential and thermal energies is given by

$$\frac{V_0}{k_B T} = \frac{q_e^2 n_{ad}}{\epsilon \epsilon_0 k k_B T}, \quad (\text{A29})$$

where n_{ad} is the typical density of adsorbed surface ions and is $n \sim 10^{13} \text{ m}^{-2}$. We find that $V_0/k_B T = 0.0018$ which gives $\exp(-V_0/k_B T) = 0.998 \sim 1$. This shows that the thermal (kinetic) energy dominates over the effective repulsive potential created by the adsorbed ions. The domination of thermal energy only takes place because of the strong screening present in the surface water layer. This result makes Eq. (A27) equivalent with Eq. (2) in Chapter 3 which was derived without electrostatic potential.

**APPENDIX B: DERIVATION OF THE MODEL EQUATION INCLUDING
THE VIBRATIONAL PARTITION FUNCTION**

The energy of a harmonic oscillator is given by

$$E_n = \left(n + \frac{1}{2}\right)h\nu. \quad (\text{B1})$$

The vibrational partition function can be written as

$$z_{vib} = \sum_{n=0}^{\infty} \exp\left(-\frac{\left(n + \frac{1}{2}\right)h\nu}{k_B T}\right) = \exp\left(-\frac{h\nu}{2k_B T}\right) \sum_{n=0}^{\infty} \exp\left(-\frac{nh\nu}{k_B T}\right). \quad (\text{B2})$$

We can make use of the relation

$$\frac{1}{1 \pm x} = 1 \mp x + x^2 \mp x^3 \dots \quad (\text{B3})$$

and let $x = e^{-h\nu/k_B T}$. This allows Eq. (B2) to be written in a finite form.

$$z_{vib} = \frac{\exp\left(-\frac{h\nu}{2k_B T}\right)}{1 - \exp\left(-\frac{h\nu}{k_B T}\right)}. \quad (\text{B4})$$

Revisiting the surface phase partition function including Eq. (B4) we have

$$z(n, T) = \binom{N}{n} z_{vib} \exp\left(\frac{n\mathbf{x}_0}{k_B T}\right). \quad (\text{B5})$$

The grand potential function is now

$$Z_G = \sum_{n=0}^N \frac{N!}{(N-n)!n!} (z_{vib})^n \exp\left(\frac{n(\mathbf{x}_0 + \mathbf{m}_s)}{k_B T}\right). \quad (\text{B6})$$

As in Appendix A, Eq. (B6) can be written in a finite form.

$$Z_G = \left(1 + z_{vib} \exp\left(\frac{(\mathbf{x}_0 + \mathbf{m}_s)}{k_B T}\right)\right)^N. \quad (\text{B7})$$

Writing the grand potential energy as before in Appendix A and taking the partial derivative, we get for n

$$n = N \frac{z_{vib} \exp\left(\frac{(\mathbf{x}_0 + \mathbf{m}_s)/k_B T}{k_B T}\right)}{1 + \exp\left(\frac{(\mathbf{x}_0 + \mathbf{m}_s)/k_B T}{k_B T}\right)}. \quad (\text{B8})$$

Solving Eq. (B8) for the chemical potential gives

$$\mathbf{m}_s = -k_B T \ln \left[\left(\frac{N}{n} - 1 \right) z_{vib} \right] - \mathbf{x}_0. \quad (\text{B9})$$

Equating Eq. (B9) with Eq. (A17) and solving for n gives

$$n = N \frac{1}{\left(\frac{k_B T}{I^3} \right) \left(\frac{\exp\left(-V_0/k_B T\right)}{P} \right) \frac{\exp\left(-\mathbf{x}_0/k_B T\right)}{z_{vib}} + 1}. \quad (\text{B10})$$

Using Gauss's law for singly ionized particles we get the model equation modified with the inclusion of z_{vib} .

$$\mathbf{s} = N \frac{q_e}{A} \frac{1}{\left(\frac{k_B T}{I^3} \right) \left(\frac{\exp\left(-V_0/k_B T\right)}{P} \right) \frac{\exp\left(x_0/k_B T\right)}{z_{vib}} + 1}. \quad (\text{B11})$$

In dimensionless form, Eq. (B11) can be written

$$\frac{\mathbf{s}}{\mathbf{s}_0} = \frac{1}{1 + \frac{P_0}{z_{vib} P}}, \quad (\text{B12})$$

which is Eq. (6) in chapter 3.

LIST OF REFERENCES

- [1] J. Cross, *Electrostatics: Problems, Principles, and Applications*, (IOP Publishing, 1987).
- [2] W. R. Harper, *Contact and Frictional Electrification* (Laplacian Press, 1998).
- [3] T. J. Fabish and C. B. Duke, *Molecular Charge States and Contact Charge Exchange in Polymers*, Jour. Appl. Phys. **48**, No. 10, p. 4256 (1977).
- [4] J. Lowell and A. C. Rose-Innes, *Contact Electrification*, *Advances in Physics* **29**, No. 6, p. 947 (1980).
- [5] D. K. Davies, *Examination of the Electrical Properties of Insulators by Surface Charge Measurements*, J. Sci. Instrum., **44** 521-4 (1967).
- [6] D. A. Seanor, *Polymer Science*, Vol. 2, ed. A. D. Jenkins, (Amsterdam: North-Holland), p. 1187, 1972.
- [7] R. G. Cunningham and H. P. Hood, *The Relationship Between Contact Charging and Surface Potential Difference*, J. Colloid and Interface Sci. **32** 373-6.
- [8] J. Lowell, *The Electrification of Polymers by Metals*, J. Phys. D: Appl. Phys. **9**, p. 1571 (1976).
- [9] H. A. Mizes, E. M. Conwell, and D. P. Salamida, *Direct Observation of Ion Transfer in Contact Charging Between a Metal and a Polymer*, App. Phys. Lett. **56** (16) (1990).
- [10] T. Shinbrot, *A look at Charging Mechanisms*, Journal of Electrostatics, **17** p. 113 (1985).
- [11] M. I. Kornfeld, *Frictional Electrification*, J. Phys. D, **9**, p. 1183 (1976).
- [12] A. W. Adamson and A. P. Gast, *Physical Chemistry of Surfaces*, 6th ed. (Wiley, 1997).
- [13] H. Freundlich, *Colloid and Capillary Chemistry*, 3rd ed., (Methuen London, 1926).
- [14] T. Matsuyama and H. Yamamoto, *Charge Relaxation Process Dominates Contact Charging of a Particle in Atmospheric Conditions*, J. Phys. D Appl. Phys. **28**, p. 2418 (1995).

- [15] F. Paschen, *Wied. Ann.*, **37**, 69, (1889).
- [16] A. Von Hippel, *Molecular Science and Molecular Engineering*, (MIT Press, Wiley & Sons, 1959)
- [17] D. Gorman, *Triboelectricity with Insulators*, Summer Student Project Presentation, NASA, Kennedy Space Center, Testbed Technology Branch, YA-C2-T, (2002).
- [18] M. D. Hogue, C. R. Buhler, C. I. Calle, W. Luo, E. E. Groop, T. Matsuyama, *Insulator – Insulator contact charging and its Relationship to Atmospheric Pressure*, *J. Electrostat.* **61** (3-4) p. 259 (2004).
- [19] M. D. Hogue, E. R. Mucciolo, C. I. Calle, and C. R. Buhler, *Two-Phase Equilibrium Model of Insulator – Insulator Contact Charging with Electrostatic Potential*, *J. Electrostat.* **63** p. 179 (2005).
- [19A] M. D. Hogue, E. R. Mucciolo, C. I. Calle, and P. E. Hintze, *Insulator Surface Charge as a Function of Pressure: Theory and Simulation*, Proceedings of the ESA Annual Meeting, p. 175 (2005).
- [19B] M. D. Hogue, C. I. Calle, C. R. Buhler, and E. R. Mucciolo, *Partial Model of Insulator/Insulator Contact Charging*, NASA Tech Briefs, Vol. **29**, No. 9, p.78, (September, 2005).
- [20] J. R. Waldram, *The Theory of Thermodynamics*, (Cambridge, 1985).
- [21] A. Zangwill, *Physics at Surfaces*, (Cambridge University Press, 1988), p. 206.
- [22] T. P. Straatsma, E. Apra, T. L. Windus, E. J. Bylaska, W. de Jong, S. Hirata, M. Valiev, M. T. Hackler, L. Pollack, R. J. Harrison, M. Dupuis, D. M. A. Smith, J. Nieplocha, V. Tipparaju, M. Krishnan, A. A. Auer, E. Brown, G. Cisneros, G. I. Fann, H. Fruchtl, J. Garza, K. Hirao, R. Kendall, J. A. Nichols, K. Tsemekhman, K. Wolinski, J. Anchell, D.

- Bernholdt, P. Borowski, T. Clark, D. Clerc, H. Dachsel, M. Deegan, K. Dyll, D. Elwood, E. Glendening, M. Gutowski, A. Hess, J. Jaffe, B. Johnson, J. Ju, R. Kobayashi, R. Kutteh, Z. Lin, R. Littlefield, X. Long, B. Meng, T. Nakajima, S. Niu, M. Rosing, G. Sandrone, M. Stave, H. Taylor, G. Thomas, J. van Lenthe, A. Wong, and Z. Zhang, *NWChem, A Computational Chemistry Package for Parallel Computers, Version 4.6* (Pacific Northwest National Laboratory, Richland, Washington, USA. 2004)
- [23] J. Cobine, *Gaseous Conductors: Theory and Engineering Applications*, (Dover, 1958), p. 159
- [24] T. B. Jones, Triboelectric Series, University of Rochester,
<http://www.ece.rochester.edu/~jones/demos/triboseries.html>.
- [25] D. R. Lide, *Handbook of Chemistry and Physics, 71st ed.*, (CRC Press, Boca Raton, FL, 1990), p. 12-84.
- [27] M. M. Francl, W. J. Pietro, W. J. Hehre, J. S. Binkley, M. S. Gordon, D. J. DeFrees, and J. A. Pople, *Self-consistent molecular orbital methods. XXIII. A polarization-type basis set for second-row elements*, *J. Chem Phys.* **77**, 3654 (1982).
- [28] H. J. Jensen, *Self-Organized Criticality: Emergent Complex Behavior in Physical and Biological Systems* (Cambridge University Press, 1998).
- [29] Water Quality Test Results, Cities of Titusville, FL and Cocoa, FL,
<http://www.titusville.com/depts/water/ccr04.pdf> (2004).